Optimal energy management and economic analysis of a grid-connected hybrid solar water heating system: A case of Bloemfontein, South Africa

P.A. Hohne[a,*], K. Kusakana[a], B.P. Numbi[b]

[a] Department of Electrical, Electronic and Computer Engineering, Central University of Technology, Bloemfontein, Free State, South Africa
[b] Department of Electrical Engineering, Mangosuthu University of Technology, Durban, South Africa

A B S T R A C T

In this paper, the optimal energy management of a hybrid solar electric water heater is presented. A typical medium density household is considered. Actual historic exogenous data, obtained from a weather station in the considered area is used as input for the established model.

The aim is to evaluate the energy and cost saving potential of the system, that may be achieved under time-based pricing, while maintaining a comfortable thermal level of the hot water user.

Comparisons between the operation of a thermostatically controlled traditional electric storage tank water heater and the hybrid solar electric water heater, offered an energy saving of 75.8% in the winter and 51.5% during the summer period.

A life cycle cost (LCC) analysis is presented, where the project lifetime is taken over 20 years. The LCC analysis of the hybrid system demonstrates a 44% saving in overall cost, as compared to a traditional water heating system. Simulation results conclude that the break-even point for the evaluated system was at R10 870 in 3.3 years, under the evaluated time-based pricing structure.

Introduction

Water heating for hygienic purposes, such as showering and bathing is one of the most energy consuming processes in residential areas. For instance, in South Africa approximately 40–60% of the total energy of a standard residential building may be allocated to the heating of water [1]. Water should be heated from a lower temperature to the user's specific comfortable thermal temperature level. Traditionally, a standard electric storage tank-water heater (ESTWH), further known as a "geyser" in South Africa, has been the foremost device for residential water heating within the country.

However, the increase in the South African population, economy and living standard, has led to an energy shortage, which has resulted in a steadily increasing electricity price. As an attempt to solve this, the main electricity supplier, Eskom, has recently introduced energy management activities, such as energy efficiency (EE) activities, and the use of renewable energy (RE) systems [2].

Since electrically supplied water heaters are of the most energy-intensive processes in residential areas, energy conservation educational material was made available by Eskom, to mitigate the unnecessarily large usage of energy by these systems [3,4]. These conservation practices include: lowering the thermostat temperature of the ESTWH for standby energy loss reduction; insulating the hot water storage tank and conduits, leading to points of hot water consumption, in order to increase thermal resistance; decreasing shower times and minimizing the hot water used for hygiene purposes [5–8].

Other educational material, released by Eskom, focused on conveying the message of switching the ESTWH off during peak energy usage periods, through the South African broadcasting network. This resulted in shifting high load demands to standard and off-peak energy usage periods and had no energy saving benefits to offer [9,10]. This, nevertheless, presented savings in costs when applied to a household subjected to time-based pricing. The method of reducing peak demands is known as demand-side management (DSM). DSM activities assist in preventing the national energy consumption to exceed the total generation capacity of the electricity supplier. If the supplier experienced a scenario where further energy was demanded than could be generated, the national electricity grid would be forced to shut down, which would be disastrous to the citizens of the country [11–13]. It could take several weeks to recover from this nationwide shut down [14,15].

Research on demand-side management (DSM) strategies, as in [16–18], on residential water heaters focusing on peak load shifting techniques, have presented promising results. These techniques make use of a timer-based control system, to shift the peak load demand to
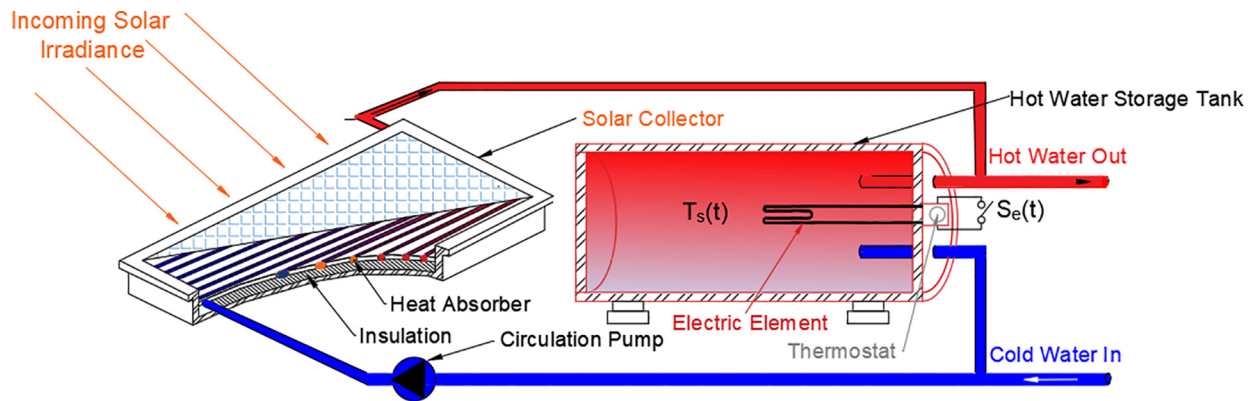
Fig. 1. SWH/ESTWH system layout.

off-peak periods with successful water temperature retention. Carefully designed DSM programs could present a possibility in having the switch-on intervals limited to once or twice a day, at minimized durations [19]. Similarly, autonomous optimal control of water heaters, based on DSM, may increase savings in cost. This DSM technique may deliver the absolute maximum savings possible, for a given water heater system, with a determined hot water consumption profile into consideration [20].

Other incentives, implemented by the electricity supplier, include rebates on the installation of renewable source water heating systems, therefore eliminating the need for electrically supplied water heaters altogether [21]. However, the replacement of electrical water heaters has the drawback of reduced hot water availability [22]. A way to disregard this drawback, is to combine the renewable energy source water heater to a backup electrically supplied water heater, compensating for the loss in hot water availability. This type of system, also referred to as a hybrid water heating system, has proven to be highly effective in reducing energy usage and costs, in the long run [23].

Energy savings, achieved with the use of hybrid renewable energy systems in conjunction with energy efficiency activities, have seen increased popularity through recent years [24]. The most popular hybrid system implemented across the world, is a solar collector coupled to an ESTWH. This system provides hot water throughout the day. Unfortunately, this too has a drawback, in terms of hot water being produced at times when it is not required, which results in excessive energy consumption [25]. As a solution to this, a hybrid water heating system, with an optimal energy control scheme is proposed ensuring maximum energy savings while maintaining the consumer's comfortable thermal level [26,27]. The solar water heater (SWH), specifically the flat plate collector, coupled to an electric storage tank water heater (ESTWH) is concluded to be the most feasible. This feasibility is based on hot water availability and cost saving being the top concern of consumers. The flat plate collector type is approximately 30% less costly to install, compared to the evacuated tube collector. Furthermore, studies suggest that sufficient solar energy is captured, to maintain a comfortable temperature level, even with a 10% less efficient heat absorbance factor, compared to the ETC [28]. In addition, the evacuated tube collector array system is costly to replace in the event of damage caused by hail, whereas, primarily the glass pane over the flat plate collector requires to be replaced, at a minimal cost, for the same instance.

The impact resistance of glass covers for the FPC system have improved in recent years, with the advent of superior glass hardening techniques [29]. This, in turn, reduces the probability of hail damage to the collector cover. The sole major drawback of the flat plate collector, is lower frost resistance in colder climates. This is particularly true for the direct collector systems. In retrospect, the indirect FPC, coupled to an ESTWH, is proposed for the South African case, taking the country's climate into consideration. The amount of solar radiation that the country receives, enables it to be an ideal water heater system for all

provinces [30].

In addition, according to the World Health Organization (WHO), the water temperature should reach 60 °C, at least once a day, to mitigate the risk of contracting Legionnaires disease. This disease is caused by a natural aquatic bacterium, generally observed in water with temperatures ranging from 20 °C to 50 °C.

Low-income households may benefit from Eskom rebates to implement these systems. The ESTWH part may assist in the prevention of infection by heating water to 60 °C daily [31].

The consumers should be able to implement a system that suits their geographical and hot water requirements, the suitable financial support from the governing body, to reduce the use and dependency on fossil fuels.

Energy efficient systems, with applicable knowledge of the advantages these systems, may offer a decrease in the severity of the energy crisis that South Africa is facing. This should, in turn, allow South Africans to improve their financial condition.

This paper is organized as follows: Section "Model development" presents the optimal control model of a hybrid indirect flat plate solar/electric water heater; Section "Data acquisition" describes the data for the case study used in this work. The baseline model is presented in Section "Baseline water heater". Simulation results of the optimally controlled hybrid solar water heater (HSWH) are discussed in Section "Results and discussion", with the aim of evaluating the effectiveness of the developed model. The economic analysis of the system is given in Section "Economic analysis". Lastly, the Section "Conclusion" serves to provide a summary of the study.

Model development

System description

The proposed hybrid system consists of an electric storage tank water heater and an indirect flat plate solar collector, as shown in Fig. 1. The solar collector is accompanied by a circulation pump to aid in the flow of water through the system. The mathematical models of the various components in the system, in terms of heat and electrical energy, is presented.

Dynamic model of the hybrid solar/electric water heating system

All the factors, in regards to the operation of the proposed hybrid water heater, should be taken into consideration if a mathematical model is to be developed.

Firstly, referring to Fig. 1, the cold water is supplied from the mains and enters the thermal storage tank. For modelling purposes, the temperature distribution of the hot water inside the storage tank is assumed to be uniform in a constant water volume, neglecting stratification [32].

In Fig. 1, the complete water heating system is illustrated, which

includes an indirect flat plat collector (FPC), with a heat exchanger located inside the collector. The FPC is coupled to an electric storage tank water heater with a single water heating element. The circulation pump in the collector arrangement operates automatically and may be seen as an independent system. The pump is controlled by a temperature differential control circuit. This control circuit monitors the temperature difference between the cold-water inlet and hot water outlet of the collector. When the temperature difference reaches a certain value, the circulation pump is switched ON. This system ensures that when solar irradiance is absent or insufficient, the pump remains OFF, so that cold water is not continuously being circulated through the storage tank. This is a necessity in preventing a decrease of the thermal level of the water supplied to the consumer.

All thermal gains and losses in the system are calculated, in order to form an energy balance equation. The energy gain calculations are discussed, followed by the losses in the system. In order to calculate the primary energy gain (energy gained from solar irradiance), all input variables should be found, as well as their coefficients.

The electrically supplied water heating system serves as an auxiliary heater, to increase hot water availability. Therefore, if the solar energy supply is ineffective in heating water, the electric resistive element will switch ON. The solar thermal energy is dependent on several factors: time of year (season), weather and time of day.

The presence of transient phenomena can be omitted or neglected from the model given the time scale of the analysis.

The difference in temperature between the cold and hot water supplied to and from the collector, may be calculated by obtaining the heat energy gained by the collector as shown in Eq. (1). Therefore, the heat gain may be calculated, in terms of the temperature differential of the water between the collector inlet and outlet as follows [33]:

$$Q_{coll} = m_c(t)c(T_{co}(t) - T_{ci}(t)) \tag{1}$$

where

Q_{coll} is the heat gained by the collector (J),
$m_c(t)$ is the variable flow rate of the water inside the collector (kg/h),
c is the heat capacity of the water inside the collector ($4184 J/kg/°C$),
$T_{co}(t)$ is the variable collector water output temperature (°C),
$T_{ci}(t)$ is the variable collector water input temperature (°C),

Due to large degrees of thermal stratification, $T_{ci}(t)$ is considered to be equal to $T_m(t)$, this gives Eq. (2):

$$Q_{coll} = m_c(t)c(T_{co}(t) - T_m(t)) \tag{2}$$

Similarly, the heat gain may be calculated, in terms of solar irradiance absorbed by the collector. The total hourly solar radiation absorbed by the collector may be evaluated, utilizing the isotropic diffuse model in Eq. (3) [34,35].

$$G(t) = G_{DNI}\cos\theta_\beta + G_{DHI}\left[\frac{1 + \cos(\beta_{coll})}{2}\right] + G_{GHI}\rho_g\left[\frac{1 - \cos(\beta_{coll})}{2}\right] \tag{3}$$

where

$G(t)$ is the variable total hourly solar radiation on a tilted collector (W/m^2),
G_{DNI} is the horizontal beam radiation (W/m^2),
G_{DHI} is the horizontal diffuse radiation (W/m^2),
G_{GHI} is the horizontal global radiation (W/m^2),
θ_β is the incidence angle on a tilted surface (°),
β_{coll} is the slope of the collector array (°),
ρ_g is the ground reflectance ($-$).

The total hourly solar irradiation may further be used in Eq. (4), [35,36]

$$Q_{coll} = A_c[F_R(\tau\alpha)G(t)t_{(h)} - F_R U_L(T_{co}(t) - T_m(t))] \tag{4}$$

where

A_c is the area of the collector (m^2),
F_R is the collector heat removal factor,
$\tau\alpha$ is the transmittance absorbance product,
$G(t)$ is the variable global solar irradiance absorbed by the collector (W/m^2),
$t_{(h)}$ is the time ($3600s$),
U_L is the collector overall heat transfer coefficient ($W/m^2 . °C$),
$T_a(t)$ is the variable ambient temperature (°C).

The collector heat gain equations (Eq. (2) and Eq. (4)) is equated so that Eq. (5) will be:

$$m_c(t)c(T_{co}(t) - T_m(t)) = A_c[F_R(\tau\alpha)G(t)t_{(h)} - F_R U_L(T_{co}(t) - T_m(t))] \tag{5}$$

The temperature difference between the hot water out and the cold water in $(T_{co}(t) - T_m(t))$ of the collector, after the heat exchanger action have taken place, may further be calculated in Eq. (6):

$$(T_{co}(t) - T_m(t)) = \left[\frac{A_s(F_R(\tau\alpha)G(t)t_{(h)})}{m_c(t)c + A_c F_R U_L}\right] \tag{6}$$

The new collector heat gain may therefore be calculated as in Eq. (7) So that,

$$Q_{coll} = \left[\frac{A_s(F_R(\tau\alpha)G(t)t_{(h)})m_c(t)c}{m_c(t)c + A_c F_R U_L}\right] \tag{7}$$

Referring to Fig. 1, the secondary heat gain ($Q_{EL}(t)$) may be calculated as, shown in Eq. (8), adapted from [33]. The power supplied to the electric resistive element remains constant. Full rated power is supplied to the electric element when it is switched on and no power is supplied when it is switched off.

$$Q_{EL}(t) = P_{EL}t_{(h)}S_e(t) \tag{8}$$

where

$Q_{EL}(t)$ is the variable heat gain from the electric resistive element (J),
P_{EL} is the full rated power supplied to the element (W),
$t_{(h)}$ is the time ($3600s$),
$S_e(t)$ is the variable switching state of electric resistive electric element ($-$).

The energy losses, due to hot water demand ($Q_D(t)$) and convectional (standby) loss ($Q_L(t)$), may be calculated, using Eqs. (9) and (10) respectively.

The standby losses, $Q_L(t)$, represent power losses through the casing material surface conduction [36].

$$Q_L(t) = U_s t_{(h)}A_s(T_s(t) - T_a(t)) \tag{9}$$

where

U_s is the heat loss coefficient of a storage tank ($W/m^2 . °C$),
A_s is the area of the storage tank (m^2),
$t_{(h)}$ is the time (3600 s),
$T_s(t)$ is the variable temperature of the water inside the storage tank (°C),
$T_a(t)$ is the variable ambient temperature of the surrounding air (°C).

The hot water demand loss ($Q_D(t)$) occurs when hot water is drawn by the consumer. Consequently, when hot water is required, the hot water demand flow rate is initiated and $T_s(t)$ drops, due to cold water flowing into tank. The cold water flows into the tank in order to

maintain a constant volume. Losses, due to the hot water demand, are given in Eq. (10), [37].

$$Q_D(t) = cW_D(t)(T_s(t) - T_m(t)) \qquad (10)$$

where

c is the heat capacity of water ($4184 J/kg/°C$),
$W_D(t)$ is the variable hot water demand flow rate (kg/h),
$T_m(t)$ is the variable temperature of the inlet water (°C).

The energy balance equation is described in terms of all the heat gains and losses in the system, given in Eq. (11).

$$M_s c \dot{T}_s = Q_{coll} + Q_{EL} - Q_L - Q_D \qquad (11)$$

where

M_s is the water mass inside the storage tank (kg),
c is the heat capacity of water ($4184 J/kg/°C$),
$\dot{T}_s$ is the derivative of the temperature variation of the water inside the storage tank (°C).

By substituting Eqs. (6)–(9) into Eq. (10), $M_s c_s \dot{T}_s$, can be presented in Eq. (12):

$$M_s c \dot{T}_s = \left[\frac{A_s (F_R(\tau\alpha)G(t)t_{(h)})m_c(t)c}{m_c(t)c + A_c F_R U_L} \right] + S_e Q_{EL} - cW_D(t)(T_s(t) - T_m(t))$$
$$- A_s U_s t_{(h)}(T_s(t) - T_a(t)) \qquad (12)$$

For the sake of simplicity, $\left[\frac{A_s(F_R(\tau\alpha)G(t)t_{(h)})m_c(t)c}{m_c(t)c + A_c F_R U_L} \right]$ in Eq. (12) is replaced with $Y(t)$ in Eq. (13).

$$M_s c \dot{T}_s = Y(t) + S_e Q_{EL} - cW_D(t)(T_s(t) - T_m(t)) - A_s U_s t_{(h)}(T_s(t) - T_a(t)) \qquad (13)$$

$\dot{T}_s$ is made the subject of the formula in Eq. (14).

$$\dot{T}_s = \frac{Y(t)}{M_s c} + \frac{S_e Q_{EL}}{M_s c} + \frac{cW_D(t) + A_s U_s t_{(h)}}{M_s c}(T_s(t)) + \frac{cW_D(t)T_m(t)}{M_s c}$$
$$+ \frac{A_s U_s t_{(h)}T_a(t)}{M_s c} \qquad (14)$$

Eq. (14) is divided into separate components, shown in Eqs. (15)–(17), so that a state space equation is formulated. The state space equation is converted, so that the temperature of the water inside the storage tank (state variable) to be made the subject of the formula, denoting [37]:

$$A(t) = \frac{cW_D(t) + A_s U_s t_{(h)}}{M_s c} \qquad (15)$$

$$B = \frac{Q_{EL}}{M_s c} \qquad (16)$$

$$\gamma(t) = \frac{cW_D(t)T_m(t)}{M_s c} + \frac{A_s U_s t_{(h)}T_a(t)}{M_s c} + \frac{Y(t)}{M_s c} \qquad (17)$$

$$\dot{T}_s = -A(t)T_s(t) + BS_e(t) + \gamma(t) \qquad (18)$$

In the state space equation given by Eq. (18), the control or decision variable is $S_e(t)$, whilst the state variable is $\dot{T}_s$ and the disturbance variable in the system is $\gamma(t)$.

Discretized hot water temperature

Eq. (18) is a continuous function which has an infinite number of degrees of freedom and needs to be transferred into a general discrete formulation in terms of the kth hot water function. This inevitably limits the degrees of freedom. The limitation is required due to the finite nature of the subsequent calculation processes. Function spaces, necessary to produce all solutions possible for given initial and boundary conditions, have an infinite dimension. Therefore, discretization is required to obtain a function space where realistic finite number of base functions containing suitable approximations of the analytical solution can be calculated.

$$T_{k+1} = T_k(1 - t_s A_k) + t_s B S_{e_k} + t_s \gamma_k \qquad (19)$$

T_k in Eq. (19) is the temperature variation inside the storage tank.

Since the state variable, T_{k+1} should be expressed in terms of its initial value, T_0 and the control variable, S_{e_k}, T_{k+1} at each interval is firstly derived as:

When substituting $k = 0$, then T_1 in Eq. (19) becomes Eq. (20):

$$T_1 = T_0(1 - t_s A_0) + t_s B S_{e_0} + t_s \gamma_0 \qquad (20)$$

Similarly, when $k = 1$, then T_2 is given in Eq. (21):

$$T_2 = T_1(1 - t_s A_1) + t_s B S_{e_1} + t_s \gamma_1 \qquad (21)$$

Substitute T_1 in Eq. (20) into Eq. (21) so that Eq. (22):

$$T_2 = [T_0(1 - t_s A_1) + t_s B S_{e_0} + t_s \gamma_0](1 - t_s A_1) + t_s B S_{e_1} + t_s \gamma_1 \qquad (22)$$

After expansion and factorization, T_2 will become Eq. (23):

$$T_2 = T_0[(1 - t_s A_0)(1 - t_s A_1)] + t_s B[(1 - t_s A_1)S_{e_0} + S_{e_1}]$$
$$+ t_s[(1 - t_s A_1)\gamma_0 + \gamma_1] \qquad (23)$$

Following the same steps taken for Eqs. (21)–(23) after $k = 2$, T_3 will then become Eq. (24):

$$T_3 = [(1 - t_s A_0)(1 - t_s A_1)(1 - t_s A_2)] + t_s B[(1 - t_s A_1)(1 - t_s A_2)S_{e_0}$$
$$+ (1 - t_s A_2)S_{e_1} + S_{e_2}] +$$
$$t_s[(1 + t_s A_1)(1 + t_s A_2)\gamma_1 + \gamma_2] \qquad (24)$$

$$T_{(k+1)} = T_0 \prod_{j=0}^{k}(1 - t_s A_j) + t_s B \sum_{j=0}^{k} S_{e_j} \prod_{i=j+1}^{k}(1 - t_s A_i)$$
$$+ t_s \sum_{j=0}^{k} \gamma_j \prod_{j=i+1}^{k}(1 - t_s A_i) \qquad (25)$$

where

T_0 and T_k are the initial and k^{th} hot water temperatures inside the tank respectively (°C),
t_s is the sampling time (s),
S_{e_k} are the switching status with single binary values (1 or 0).

Optimization control problem

Operation cost minimization

The primary objective is to minimize the cost of energy supplied to the electric resistive element. In order to accomplish this, most of the control switching-ON should take place in off-peak periods. When switching-ON during off-peak periods, the cost of electrical energy should be significantly reduced. The Eskom 2017/2018 TOU tariff periods [38], are represented by Fig. 2.

The tariff circle chart on the left represents the TOU tariff periods of the low demand season, whereas the circle chart on the right, denotes the periods of the high demand season.

The low demand season is from September to May, whilst the high demand season begins in June and ends in August. The winter season peak period starts an hour earlier than the summer season. This may be accredited to increased energy requirement to heat water to the desired temperature and the usage of other high energy consumption appliances, such as space heaters.

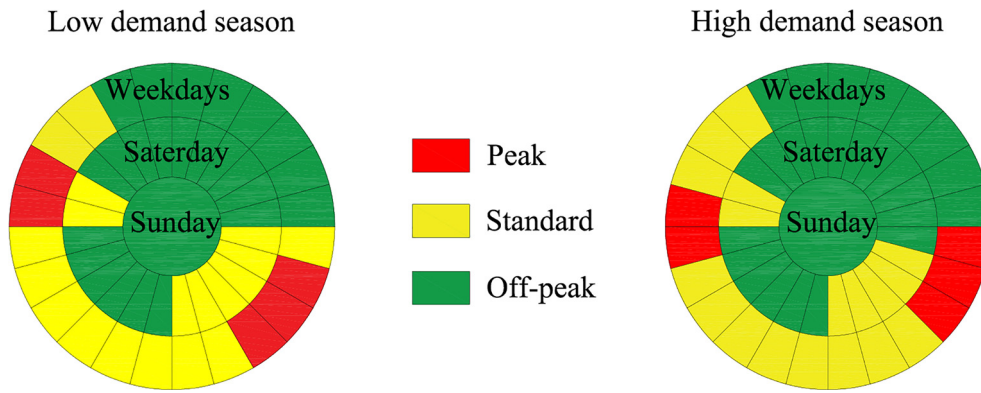The TOU tariff structure forms a substantial part of the primary

Low demand season

High demand season

Fig. 2. Time-of-Use Periods [38].

objective function and is derived in Eq. (26), which is the electricity cost J_p minimization [37]. The switching function, S_{e_k}, is therefore highly dependent on the TOU tariff.

$$J_p = t_s P_{EL} \int_{t_0}^{N} p_t S_{e_t} \qquad (26)$$

where

t_s is the sampling time (h),
p_k is the TOU tariff function (R/kWh),
P_{EL} is the rated power of the electric resistive element (W),
S_{e_k} is the switching status function of the element (–).

Thermal discomfort level minimization

The level of thermal discomfort may be defined by the experience of the user, once the temperature levels of the hot water are above or below the desired temperature. The discomfort level is reduced or minimized, when the thermal level reaches the desired hot water temperature. The secondary objective, therefore, becomes the minimization of thermal discomfort experienced by the user. In order to know when the desired temperature should be reached, a user specific load profile is evaluated. The load profile is a continuous function, represented by $F(t)$ and denotes the desired hot water temperature of the user. $T_s(t)$ is the temperature of the water inside the storage tank and should be close, or equal, to the desired temperature at the time when hot water is required.

In other words, the difference between $F(t)$ and $T_s(t)$ should be as small as possible, at the precise time when hot water is usually drawn. Thus, the difference in temperature $(T_s(t) - F(t))^2$ will be minimized [39].

The secondary objective function, J_s, is shown in Eq. (27).

$$J_s = \int_{t_0}^{t_f} (T_s(t) - F(t))^2 dt \qquad (27)$$

where

t_0 is the initial sampling interval at $T_s(t) = T_s(t_0)$,
t_f is the final sampling interval at $T_s(t) = T_s(t_f)$.

Fixed-final state condition

In order to simulate continuous operation and repeated implementation of the optimal energy control strategy for the hybrid system, the thermal energy stored in the storage tank at the end of the control horizon should be equal to the thermal energy at the beginning of the control horizon. Therefore, the sum of all the energy gained should be equal to all the energy lost in the system, for the respective control horizon. This is represented in Eq. (28). The final temperature $(T(t_f))$, in the last sampling interval, should thus be equal to the initial temperature $(T(t_0))$ of the water inside the storage tank, at the initial

sampling interval of the control horizon [40].

$$\sum_{k=1}^{N} (Q_{s_k}) = 0 \qquad (28)$$

This may be achieved by minimizing the difference between the actual final temperature and the desired final temperature, which is equal to the initial temperature of the water inside the storage tank. The same method used to minimize the discomfort level of the user may be applied for this instance, as shown in Eq. (29). In this case, the difference between the final and initial temperature is minimized, so that Eq. (29) forms part of the final objective function.

$$J_t = \left(\int_{t_0}^{t_f} T(t_f) - T(t_0) \right)^2 \qquad (29)$$

Operation cost and discomfort level minimization

In order to minimize the operational cost of the solar water heater, while maintaining the thermal comfort level of the user, the primary, secondary and tertiary objective functions should be added, as shown in Eq. (30).

$$\text{Min } J = J_p + J_s + J_t \qquad (30)$$

Substituting Eqs. (26), (27) and (29) in Eq. (30), one obtains Eq. (31):

$$\text{Min } J = w_1 \left(t_s P_{EL} \int_{t_0}^{N} p_t S_{e_t} \right)$$
$$+ w_2 \left(ts \left(\int_{t_0}^{N} (T(t) - F(t))^2 dt \right) + ts \int_{t_0}^{N} (T(t_N) - T(t_0))^2 \right)^2 dt \qquad (31)$$

where

w_1 is the weighting factor to set priority to cost minimization,
w_2 is the weighting factor to set priority to cost minimization,
J is the final objective function that should be minimized.

Constraint on the state of temperature inside the storage tank

The desired temperature, when evaluating the load profile, should be between 55 °C and 65 °C at 06:30 in the morning and at 20:00 in the evening, whilst from 07:00 to 20:00, the temperature may vary, without any constraints. For repeated operation, the final temperature in the control horizon should be equal to the initial temperature. Eq. (32) shows the temperature requirements throughout a 24-hour control horizon.

$$F(t) = \begin{cases} T_s(t), & t \in [00h00, 06h00) \cup [20h30, 24h00) \\ 60, & t \in [06h30] \cup [20h00] \\ T_0(t_0), & t \in [24h00] \end{cases} \qquad (32)$$

where

$F(t)$ is the desired temperature function,

And,

$$T_s(t) = T_0 \prod_{j=0}^{k} (1 - t_s A_j) + t_s B \sum_{j=0}^{k} S_{ej} \prod_{i=j+1}^{k} (1 - t_s A_i) + t_s \sum_{j=0}^{k} \gamma_j \prod_{j=i+1}^{k} (1 - t_s A_i)$$

(33)

The switching function, S_{ek}, that is the function which describes how the electric element will switch ON or OFF, either full rated power or no power is delivered, respectively. This means that the switching status may solely be a single binary value, as illustrated in Eq. (34):

$$S_{ek} \in \{0, 1\}$$

(34)

Proposed optimization solver and algorithm

The objective function, as shown in Eq. (31), is a non-linear function, with an integer binary control variable that should be solved, in order to obtain the optimal switching status of an electric resistive element. This type of problem may be solved by the universal SCIP (Solving Constraint Integer Programs) solver, in the Matlab optimization toolbox. SCIP has further been reported to be one of the fastest solvers in the Matlab interface OPTI-Toolbox [41].

The MINLP form should be satisfied, so that SCIP may operate effectively. The form MINLP form is shown in Fig. 3. The objective function is minimized by default and is subjected to the constraints shown. The mathematical model should be rearranged, to fit the SCIP constraints, in order to solve the optimization problem. The end result is an optimal switching status function, constrained to take on a binary value.

where

$f(x)$ is the objective function,
$Ax \leqslant b$ is the linear inequality constraint,
$A_{eq}x = b_{eq}$ is the linear equality constraint,
$lb \leqslant x \leqslant ub$ is the decision variable bounds,
$c(x) \leqslant d$ is the nonlinear inequality constraint,
$c_{eq}(x) = d_{eq}$ is the nonlinear equality constraints,
x_i is an integer number decision variable,
x_j is a binary number decision variable.

The objective function is consequently replaced with $f(x)$; no linear inequality or equality constraints exist. The decision variable as shown in Eq. (34), is a binary value, meaning that only a 1 or 0 may be obtained as the switching status. The lower and upper boundaries are therefore shown in Eq. (35) and Eq. (36), respectively:

$$\text{Min}_x \; f(x)$$

subject to: $Ax \leq b$

$$A_{eq}x = b_{eq}$$

$$lb \leq x \leq ub$$

$$c(x) \leq d$$

$$c_{eq}(x) = d_{eq}$$

$$x_i \in \mathbb{Z}$$

$$x_j \in \{0,1\}$$

Fig. 3. MINLP Form.

$$lb^T = [0. \, .. 0_N]$$

(35)

$$ub^T = [1. \, .. 1_N]$$

(36)

The control variable that should be optimized, is therefore constrained, as shown in Eq. (37)

$$lb \leqslant x \leqslant ub$$

(37)

Model validation

The model was verified using data originating from similar studies, previously conducted. The study considered simulation [42] and experimental results [43]. Comparisons, in all aspects of temperature change as a result of varying the control variable in the system, with regards to all associated heat losses and gains, have presented small margins of error [44].

Economic analysis

Cumulative energy cost

In order to calculate the daily cumulative energy cost, the primary objective function in Eq. (26) may be adapted from Section "Optimization control problem" so that Eq. (38) will be:

$$C_{daily-EC} = t_s. \, P_{EL} \sum_{k=1}^{N} (C_{TOUk}. \, S_{ek})$$

(38)

where

t_s is the sampling time,
P_{EL} is the rated power of the electric resistive element ($3 \, kW$),
C_{TOUk} is the time-based cost of electricity at each kth interval in ZAR/kWh,
S_{ek} is the switching status of the electric resistive element,

Cumulative replacement cost

The cumulative replacement costs of the system components (C_{rep}) at the end of the project lifetime, may be calculated, using Eq. (39):

$$C_{rep} = \sum_{k=1}^{N_{rep}} C_{cap}. \, k(1 + n. \, r)$$

(39)

where

C_{cap} is the initial capital cost for each component.
N_{rep} is the number of component replacements of the project lifetime,
n is the lifespan for a specific component (years),
r is the historic average inflation rate,
k represents each year in the project lifetime.

Operation and maintenance costs

The operation and maintenance costs at the end of year one ($C_{OM-initial}$) of the system, may be taken as 1% of the initial implementation cost. The total operation and maintenance cost (C_{OM}), over the project lifetime, may be obtained, using Eq. (40):

$$C_{OM} = \sum_{k=1}^{N} C_{initial-OM}. \, k(1 + r)$$

(40)

where

$C_{initial-OM}$ is the operation and maintenance cost for the first year.
k represents each year in the project lifetime,
N is the number of years in the project lifetime,
n is the lifespan for a specific component (years),
r is the 10% annual energy price increase.

Salvage costs

In the event where future upgrades are required after the project lifetime has been reached, the system may be salvaged and sold at the salvage cost. The salvage cost ($C_{salvage}$) may be taken as 20% of the initial implementation cost ($C_{initial}$) of the system, as shown in Eq. (41).

$$C_{salvage} = 0.2 \cdot C_{initial} \tag{41}$$

Total life cycle cost

The total lifecycle cost of the system may be calculated, by adding the costs in Eqs. ((38)–(41)), the subtraction of the salvage cost ($C_{salvage}$) and addition of energy costs incurred (C_{EC}), as represented in Eq. (42):

$$LCC = C_{initial} + C_{rep} + C_{EC} + C_{OM} - C_{salvage} \tag{42}$$

Data acquisition

The case represents a traditional medium density household, with 3 occupants located in Bloemfontein, Free-state, South Africa. The average daily hot water demand flow rate, solar irradiance, inlet water temperature and ambient temperature, retrieved on an hourly basis from the selected site, are shown in Figs. 4–12. In Figs. 4–9 the average data for the annual seasonal extremes, namely winter and summer, is presented, in order to highlight the variation throughout the average day. Figs. 10–12 include the monthly averages calculated for remaining months of the year, for all the variable data presented in Figs. 4–9.

Diffuse horizontal, diffuse normal, global horizontal irradiance and ambient air temperature of an average winter day in July and an average summer day in January, are plotted in Figs. 5–6 and Figs. 8–9, respectively. The daily data was collected from the weather station, located at the University of the Free-State (latitude: −29.11074, longitude: 26.18503 and elevation: 1491 m) in Bloemfontein [45].

The ambient and water inlet temperature, represented in Figs. 5 and 8, for the average winter day in July and summer day in January, are presented, respectively. The ambient temperature deviates significantly with time when compared to the inlet water temperature. No minute or hour averaged data for inlet water temperature exists for the case study area, meaning that the inlet water temperature should be based on assumptions. The median water temperatures obtained once per season, retrieved from [46], were used for the case study. The median inlet water temperatures of winter and summer, were taken as 13.3 °C and 23.1 °C, respectively. Merely small changes in temperature may be assumed for the inlet water. The approximations were made, based on the heat capacity of water and air, combined with the fact that most of the city's water conduits are buried beneath the ground. Fluctuations in ground temperature are significantly lower, when compared to air temperature. This in turn reduces the influence of ambient air temperature on the inlet water temperature. The water temperatures are, therefore, assumed to be near constant, with slight delayed deviations that follow the variation in air temperature.

A 24-hour detailed average summer (January) hot water consumption profile was obtained and is shown in Fig. 9, while the winter (July) profile in Fig. 6, was adapted from [47], with reference to the summer profile. In summer, the desired temperature was obtained by adjusting the hot and cold-water taps. The flow rate of the hot water, after cold-water cut-off, was measured to be 3.23 L per minute. The showering time of the first occupant was measured to be 7 min, whilst the second and third occupants had showering times of 9 and 10 min, respectively. The times during the day at which the showers of the first 2 occupants took place, was between 06:30 and 07:30. The third occupant, as per the normal daily routine, showered at 20:00. The demands for the remaining months were approximated, based on the existing profiles and the temperature variation through the year as in [43].

Component sizes and simulation parameters

The aim of the current work is to apply an optimal energy management scheme to the hybrid water heating system. A baseline model in Section "Baseline water heater" is adapted from the hybrid water heating system model in Section "Results and discussion", so as to simulate thermostat operation, without solar irradiance as input. Rather, the sole energy input to the system will be the energy supplied from the electric resistive element. The baseline model is hence simulated with identical component sizes and input data as the hybrid system, without the influence of the collector. The component sizes and parameters of the baseline and hybrid system, are shown in Table 1-retrieved from [48–51] and adapted for South African case.

The tilt angle of the collector is taken to be 30°, due to the fact that most certified collector installers in the region usually use this angle as a rule of thumb. The solar angles of incidence were calculated for the days on which the data was taken.

The storage tank size was taken as 150 L. This choice in capacity was based on the requirements of the three occupants in the case study. The 150 L ESTWH is accompanied by a 3-kW electric resistive element.

The TOU tariff structure and pricing layout is illustrated in Table 2; the tariff is enforced by Centlec (electricity distribution and managing company for the Bloemfontein and surrounding area). From the table, the high demand season with the most costly electricity prices, falls in the winter period, which is from June to August, while the low demand season is between September and May. Additionally, the low and high demand seasons' peak, off-peak and standard periods, start and end at various hours throughout the day. The highest electricity price at R3.23, is effective in the peak period of the high demand season, while
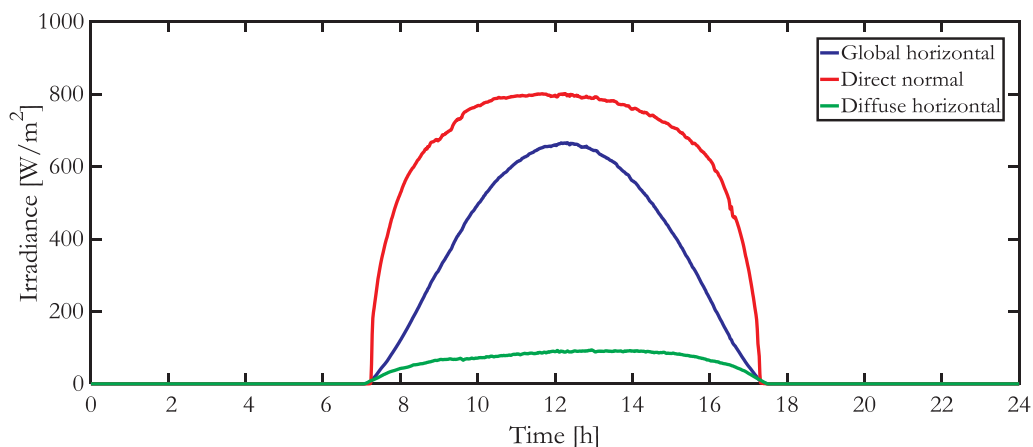

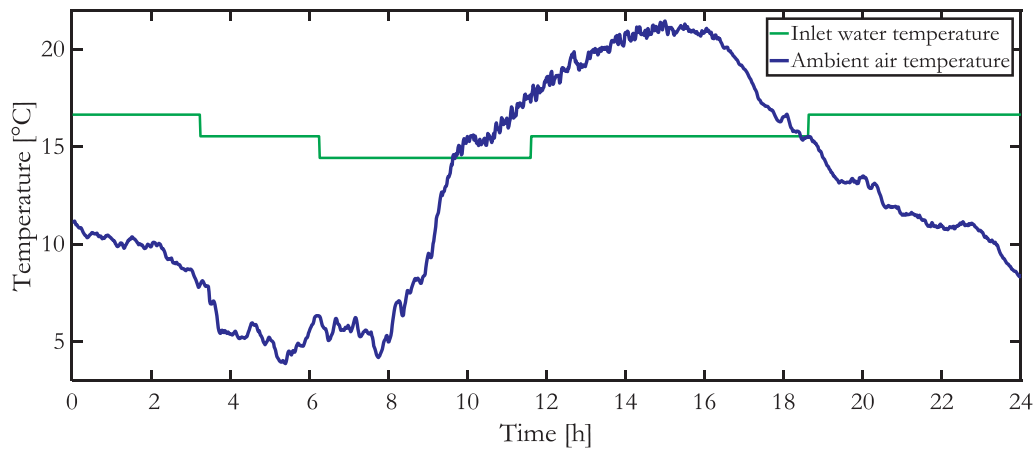**Fig. 4.** Winter solar irradiance (July 2017 average).

Fig. 5. Winter ambient and inlet water temperature (July 2017 average).

the lowest is R1.20, during the off-peak period of the low demand season. This means that there is a difference of 269%, from the lowest electricity price to the highest, for the same year [52,53].

The simulation parameters are presented in Table 3. The size of the sampling time is indirectly proportional to the time taken to simulate a certain process. Smaller sampling intervals are generally required for state variables that rapidly vary when disturbances are introduced in the system. For this study, however, the state variable is the temperature of water, which has the tendency to react in a delayed nature, compared to other processes. Due to this, and computational limitations, a 15-minute sampling interval over a control horizon of 96 (representing 24 h) was chosen in order to decrease simulation time.

Baseline water heater

In order to validate whether the optimal switching model reduces energy costs to the consumer, a baseline should be established. The baseline model is an electric storage tank water heater (ESTWH), without a solar collector. The temperature is regulated by means of a thermostat, where the default temperature is set to 65 °C. The thermostat should maintain an approximate temperature of 65 °C throughout the day, by automatically switching the electric resistive element ON and OFF, at the times when it is required. The thermostat has a temperature range of 5 °C. This means that the element will switch on to increase the thermal level when the temperature drops to the lower thermostat switch ON temperature, in this case is 60 °C.

Most electric storage tank water heaters in South Africa use the bi-metal thermostat system. This system is known to deviate from the

actual set temperatures, by an average of 3 °C. The simulation of the thermostat operation should hence stay within the 3 °C range, so that the accuracy of the baseline operation is maintained [54].

Two separate cases are simulated and illustrated, to represent the winter and summer months. The switching function of the thermostat and the associated change in water temperature inside the storage tank, is presented in Section "Baseline: Winter case" for winter and Section "Baseline: Summer case" for summer.

Baseline: Winter case

In Fig. 13, the switching function of the thermostat is presented. For a specific hot water consumption profile, inlet water temperature and ambient air temperature described in Section "Data acquisition", the switching of the electric element is concluded to take place during the peak and standard periods of the TOU tariff structure. Fig. 14 illustrates the resultant change in temperature of the water inside the storage tank due, to the switching in Fig. 13. The preferred thermal level, is concluded to be between 55 °C and 65 °C, illustrated in orange, while hot and cold is illustrated in red and blue, respectively. With the thermostat setting at 65 °C, the water temperature remains within the desired temperature even when hot water is not required. This increases the cost of electricity significantly, justifying the requirement for an optimal control approach.

When comparing the switching function to the water temperature inside the storage tank, it may be observed that the switching mainly occurs directly after the times when hot water is drawn by the occupants. This can mainly be attributed to temperature falling below the
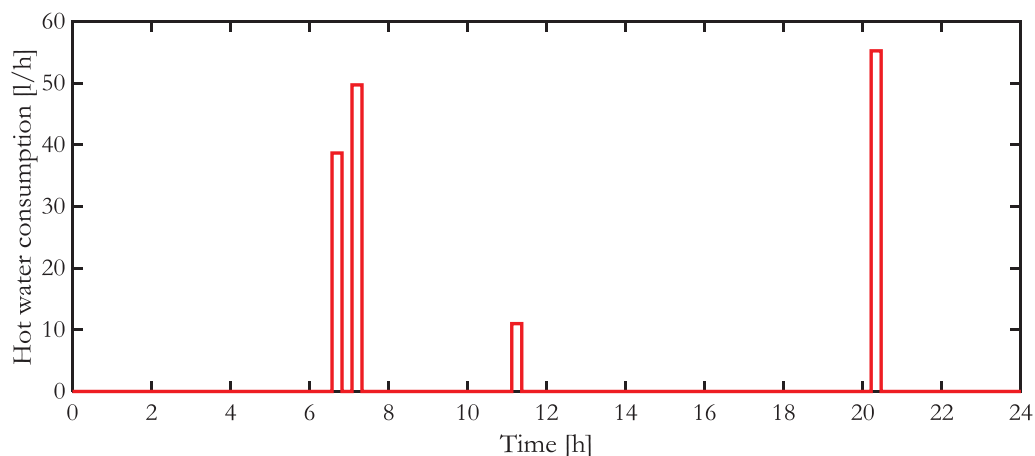

Fig. 6. Winter hot water demand i.e. flow rate (July 2017 average).
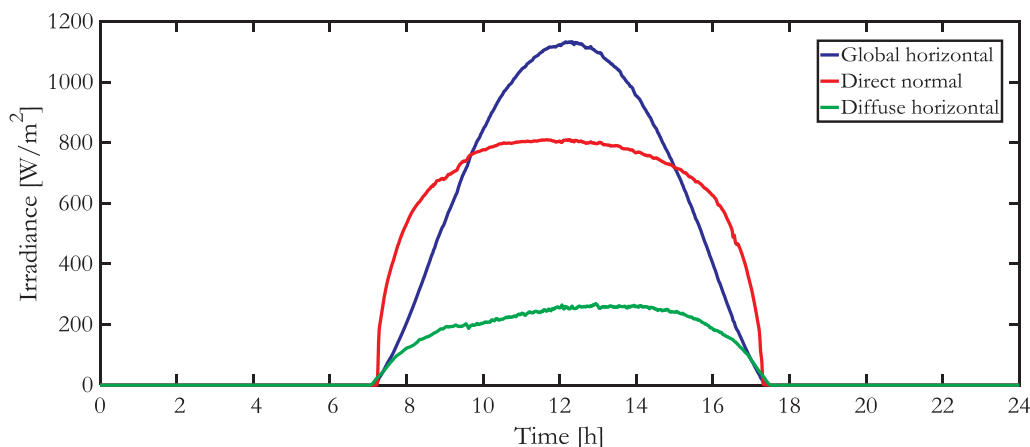
Fig. 7. Summer solar irradiance (January 2017 average).

thermostat control temperature, due to the withdrawal of hot water and the incoming cold inlet water temperature, to maintain the constant volume.

Baseline: Summer case

In Fig. 12, the switching function of the thermostat is presented. The summer input data from Section "Data acquisition" is used for this simulation. The switching-ON of the electric element is concluded to take place during the peak and standard periods of the TOU tariff structure. Fig. 16 illustrates the resultant change in temperature of the water inside the storage tank, due to the switching in Fig. 15.

Results and discussion

In this section, the operation of the proposed hybrid system, with optimal control is described. The hybrid system's optimal switching function and associated water temperature inside the storage tank, is illustrated in Section "Optimal control of the HSWH: Winter case", for the winter case and "Optimal control of the HSWH: Summer case", for the summer case. The same input data in Section "Data acquisition", is used to simulate the operation of the hybrid system with the optimal control approach.

Optimal control of the HSWH: Winter case

The optimal switching function of the HSWH (during July), is presented in Fig. 17 and the resultant temperature of the water inside the

storage tank, is presented in Fig. 18. In order to reach the desired temperature at the instant when a hot water demand occurs, switching should take place prior to this demand.

Most switching occurs during the off-peak period; at 03:45 in the morning and 23:30 in the evening. The heating element is switched ON for 15 min, so that the water temperature may reach the desired temperature at 06:30. The first occupant draws hot water; a sharp decrease of temperature is observed, while at 07:00, the water is nevertheless within the desired thermal comfort level, for the second occupant's hot water consumption routine.

The temperature of the water inside the storage tank at 07:30, when the second occupant has ended his shower, is shown to drop slightly below the comfortable level. This thermal level at 54 °C may nevertheless be seen as acceptable, if one of the first two occupants opt to take a lengthier shower. Solar radiation begins to increase the thermal level of the water inside the storage tank, at the same time-step. The temperature rises until 11:00, where it suddenly drops, due to the hot water consumed by the dishwasher or washing machine. At 11:30, the water temperature gradually rises, due to the solar irradiance supplied to the collector. At 20:00, the third occupant showers and the temperature drops due to the inflow of cold water in the storage tank, while hot water is drawn after the third occupant's hot water consumption routine, the temperature remains within the desired temperature range.

Finally, the element switches ON for the last time at 23:30, during the off-peak period, in order to maintain final fixed state conditions.

The temperature at the final sampling interval is equal to the initial temperature, so that the cycle may be repeated the next day.
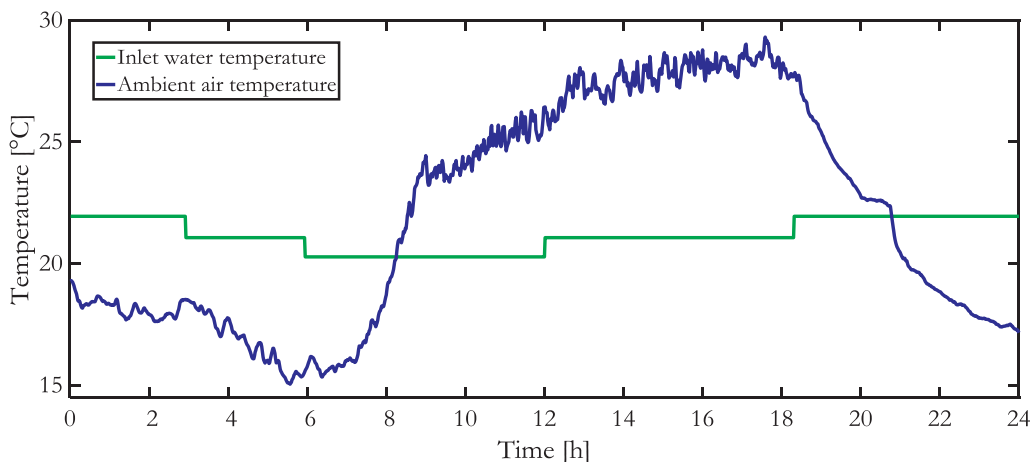

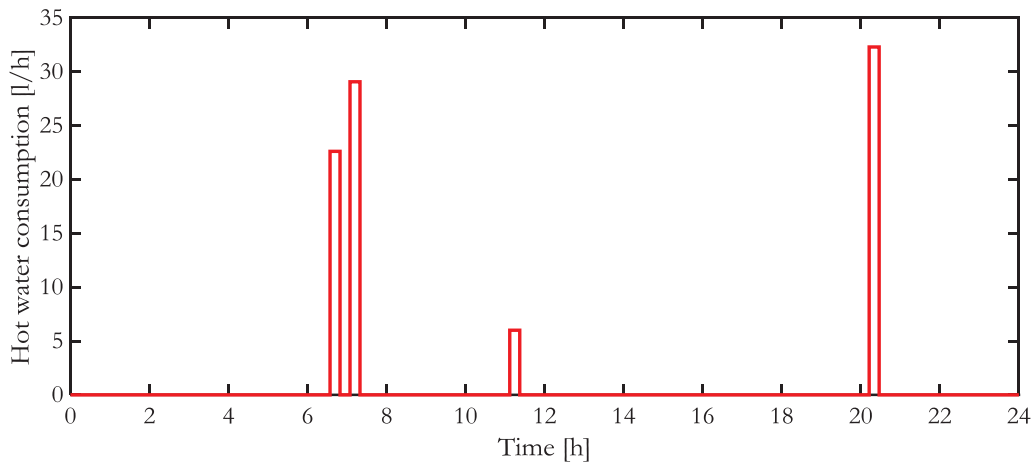**Fig. 8.** Summer ambient and inlet water temperature (January 2017 average).

Fig. 9. Summer hot water demand i.e. flow rate (January 2017 average).

Optimal control of the HSWH: Summer case

Referring to Figs. 19 and 20, switching merely takes place once at 03:00, for 15 min, in order to prepare for the first occupant's hot water demand. The switching function remains at zero throughout the rest of the control horizon. The low switching frequency during the summer period may be accredited to low hot water demand and higher ambient and inlet water temperatures, compared to the winter season. However, the angle at which the solar radiation (beam radiation) enters the collector in the summer season, is higher than that of winter. Meaning that the total effective solar irradiance absorbed by the collector, is less. The combined effect of all these factors gives rise to a storage tank water temperature, that remains within the comfortable thermal level with minimal switching required, as shown in Fig. 19. At 07:30, when the first two occupants have ended their daily hot water consumption routine, the temperature briefly falls, however, it remains within the desired range. Thereafter, the heat from the sun increases the temperature. The dishwasher/washing machine demand at 11:00 causes a slight reduction in temperature, while it is once again recovered by solar energy, up until 20:00, when the third occupant draws hot water. At 20:15, after the last demand of the day has taken place, the temperature drops down to 58.3 °C, where it decreases further, due to standby losses. At 24:00, the temperature reaches approximately 58 °C, which is equal to the initial temperature in the control horizon, to maintain fixed final state conditions.

Comparison between the baseline and optimal control of the HSWH

For both the baseline and the optimized hybrid system, the temperature of the water inside the storage tank exceeds 60 °C at least twice a day for the winter, as well as the summer case. As discussed in the "Introduction" section, this reduces the risk of contracting Legionnaire's disease, caused by the Legionella pneumophila bacteria.

It is evident that while switching the resistive element ON during off-peak periods, rather than peak or standard periods, the desired thermal level of the hot water consumer may nevertheless be maintained. The fact that the temperature remained within the preferred range for the winter case, when hot water consumption is higher in comparison, substantiates the requirement for an optimal control strategy.

All optimal control scenarios presented in the "Results and discussion" section, have been simulated with equal weighting factors so that equal priority is given to cost and discomfort minimization. For the optimal control scenario, it may be observed that all switching takes place during off-peak periods. This means that, if higher priority was given to cost minimization, the cost savings would not increase. However, if priority was given to discomfort level minimization, the result would be higher energy costs.

Economic analysis

In order to evaluate the cost effectiveness of the hybrid system in terms of money spent, several economic performance indicators exist.
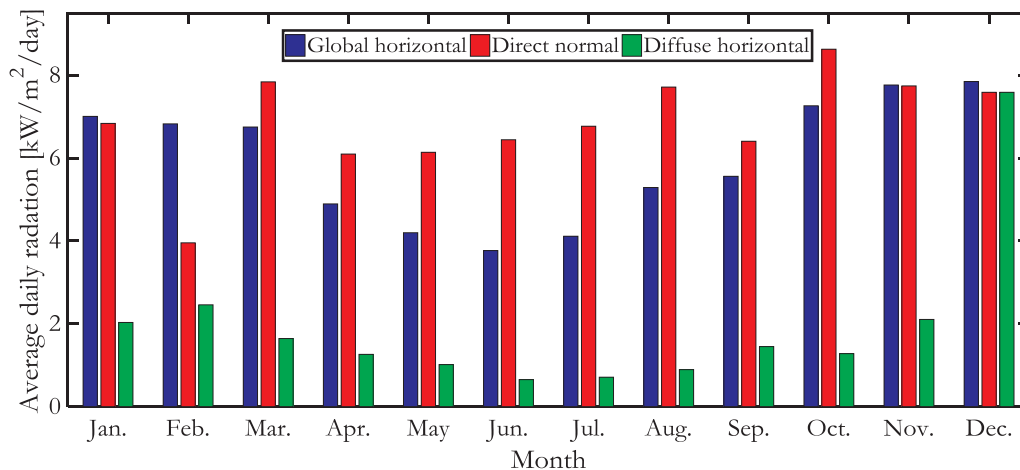

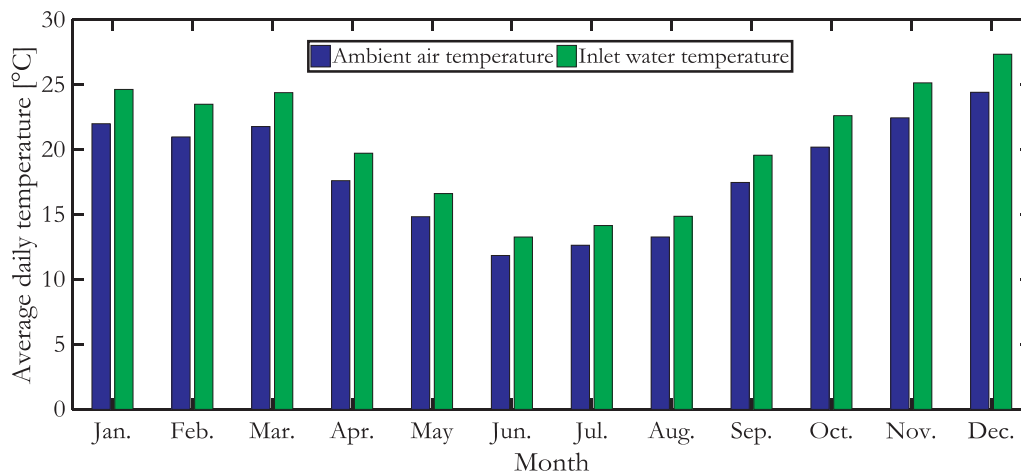**Fig. 10.** Monthly average solar irradiance (2017).

Fig. 11. Monthly average ambient air and water temperature (2017).

These indicators may include the simple payback period (SPP), life cycle cost (LCC), benefits-to-cost ratio (BCR) and initial rate of return (IRR). The SSP is the easiest to understand, due to its simplified cost calculation. However, limitations exist in the sense that it does not consider future inflation, that might affect the total cost over the life-time of a project. Another drawback of the SPP, is that it does not account cash flows beyond the payback period (PBP), as the project lifetime is not taken into consideration. This reduces the accuracy of the economic analysis and leaves investors with an approximate cost or profit prediction. With this in mind, methods such as the BCR, LCC and IRR, offer a more precise cost analysis, compared to SSP, due to the fact that inflation and project lifetime are considered [55]. Therefore, for increased accuracy, a total life cycle cost evaluation is done, followed by a break-even point (BEP) analysis, in terms of the baseline and proposed hybrid system. The life cycle costs should be compared fur-ther, to calculate the savings over a specific project lifetime. The project lifetime for this case study was determined to be 20-years.

Initial implementation cost of the proposed hybrid system

The initial investment cost of a hybrid SWH/ESTWH system, is presented in Table 4. The ESTWH and SWH combination was de-termined, due to the manufacturer being approved by the Eskom rebate programme. Furthermore, the manufacturers' products ultimately comply with Eskom and South African Bureau of Standards (SABS) criteria. The rebate reduces the total investment cost by approximately 40%. The flat plate collector listed is frost resistant, ensuring it's suit-ability for Bloemfontein's freezing temperatures in winter. In addition,

Table 1
Component sizes and parameters of the hybrid solar electric water heater.

Parameter	Description	Value
A_{coll}	Effective absorbance area of the collector (m^2)	2
A_s	Storage tank area (m^2)	1.1
β_{coll}	Tilted angle of the collector array (°)	30
C	Heat capacity of water (J/kg.°C)	4184
F_R	Heat removal factor (–)	0.6646
$m_c(t)$	Collector flow rate ($kg/s.m^2$)	0.011
M	Storage tank capacity (kg)	150
P_{EL}	Rated power of electric resistive element (W)	3000
Q_{EL}	Energy delivered to resistive element (MJ/h)	10.8
ρ_g	Ground reflectance (–)	0.2
T_d	Desired hot water temperature (°C)	60
$T_{s,max}$	Default thermostat switch-off temperature (°C)	65
T_{stat}	Thermostat switch-on temperature (°C)	60
$\theta_{\beta,s}$	Summer incidence angle on tilted surface (°)	109
$\theta_{\beta,w}$	Winter Incidence angle on titled surface (°)	67.6
$\tau\alpha$	Transmittance absorbance product (–)	0.7445
U_L	Collector overall heat transfer coefficient (W/m^2.°C)	7.28
U_s	Heat loss coefficient of storage tank (W/m^2)	0.3

the flat plate was chosen over the evacuated tube system, due to a major cost difference of approximately 30%. The prices in Table 4, obtained from [56–58], are average component prices for the year 2017.

Cumulative cost comparison

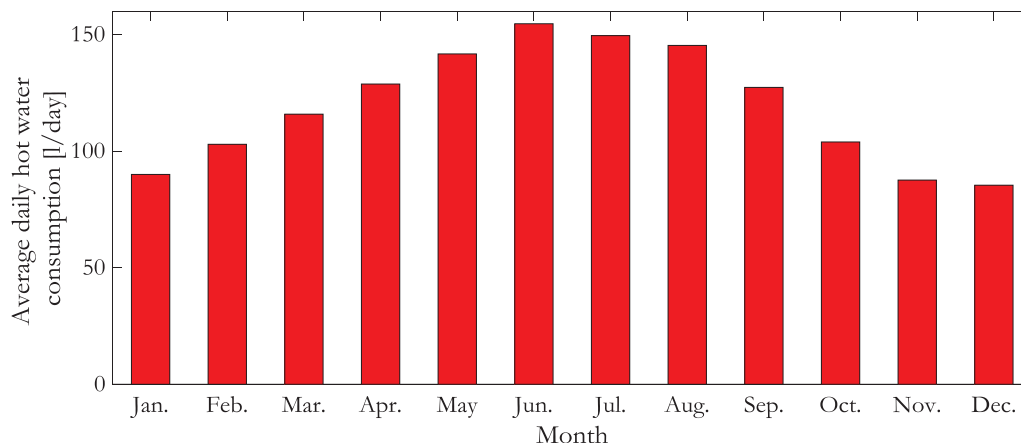Calculating the cumulative costs incurred over a specific project

Fig. 12. Monthly average hot water consumption.

Table 2
Homeflex single phase TOU tariff structure and pricing.

Season	Months	Period	Time	Rate (ZAR)
High Demand (Winter)	June-August	Off-peak	00:00–06:00, 22:00–24:00	1.7875
		Standard	09:00–17:00, 19:00–22:00	1.8643
		Peak	06:00–09:00, 17:00–19:00	3.2351
Low Demand (Summer)	September -May	Off-peak	00:00–06:00, 22:00–24:00	1.2063
		Standard	06:00–07:00, 10:00–18:00, 20:00–22:00	1.3269
		Peak	07:00–10:00, 18:00–20:00	1.7108

Table 3
Simulation parameters.

Parameter	Description	Value
t_s	Sampling time (min)	15
N	Control horizon (–)	96
Hours	Total hours in control horizon (h)	24

lifetime, in this case 20-years, a few factors should be taken into consideration. Described in the "Initial implementation cost of the proposed hybrid system" section, the initial cost of implementation may not be observed as cumulative, due to the fact that the cost implementation is a once-off amount, incurred solely at the inception of the project. With this in mind, the annual costs incurred, which includes replacement costs and operation and maintenance (O & M) costs after each year, since the starting point of the project can directly be added to the initial implementation cost, in order to obtain the total cumulative cost over the project's lifetime.

Furthermore, salvage costs at the end of the project lifetime are included, however, similar to the case of the initial cost of implementation, this cost may be observed as once-off. Moreover, the salvage cost may be deducted from the total life cycle cost and seen as a cost benefit, rather than a loss.

Winter cumulative energy cost comparison

The cumulative cost of the average winter day is presented in Fig. 21. The switching functions in Sections "Baseline water heater" and "Results and discussion" refer that, (observed from the curves), every time switching occurs, the cost of switching in the specific TOU tariff period increases the total daily cost. At the end of the control horizon at 24:00, the difference in total cost may be observed. The cumulative curves in Fig. 21 show a directly proportional relationship between the baseline and optimal control strategy. The optimally scheduled hybrid system switches ON during the off-peak period, while the baseline switching ON time is delayed by 2 h and 15 min. The baseline water

heater is effectively switched ON for 45 min during the peak period in order to maintain the thermostat temperature. This process is repeated in the evening with the sole differences being that the system is switched ON for a shorter time during the off-peak and standard Time-of-Use period. When comparing the operational cost curves at the end of the control horizon, it may be observed that the baseline's total net energy costs is approximately 4 times higher than that of the optimally scheduled hybrid system.

Summer cumulative energy cost comparison

The cumulative cost of the summer period is presented in Fig. 22. Similar to the winter cumulative cost curve in Fig. 21, the summer switching function of the baseline system follows the optimal switching curve, with a 2 h and 15-minute delay. After the first switching interval of the optimally controlled system, the curve remains constant, ensuring that the cumulative cost remains close to R1.00, for the rest of the control horizon. This is a result of the element being ON for 15 min during the off-peak period. The baseline heater and optimally controlled hybrid system, switches ON for 15 min in the morning. The cost of switching the baseline ON during the peak period in the morning, is higher than the total cumulative costs of the optimally scheduled system. The difference in cumulative energy cost, at the end of the control horizon, represents the daily energy cost savings as in the winter case. The baseline energy cost, compared to the optimal controlled system, concludes an energy cost higher by a factor of 2.5. This is significantly lower than the winter case and presents the notion that the optimal system is furthermore effective during the winter season.

Average daily energy costs

The average daily cumulative costs for the baseline and optimally controlled system for each month, are presented in Fig. 23. According to the TOU tariff structure, the high demand season is from June to August, while the low demand season is from September to May. The high demand season is illustrated in blue and the low demand season is illustrated in orange. The highest costs were incurred during the high
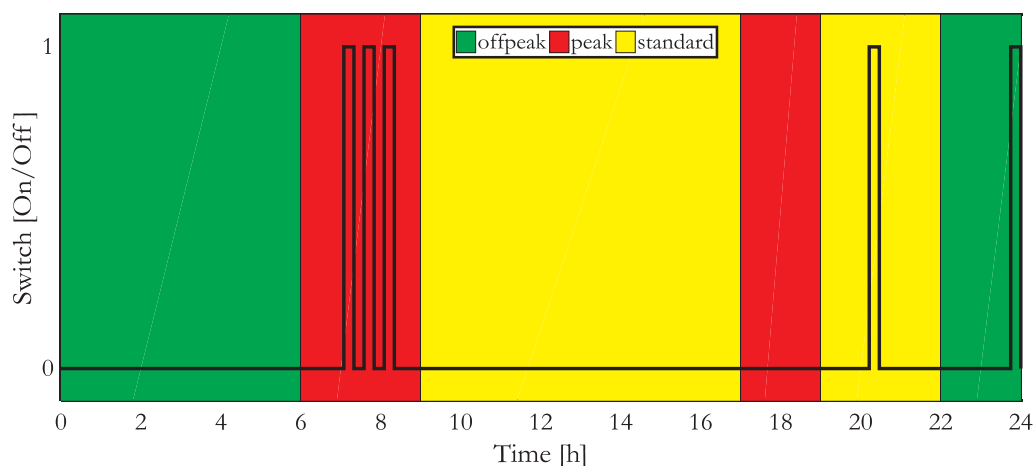

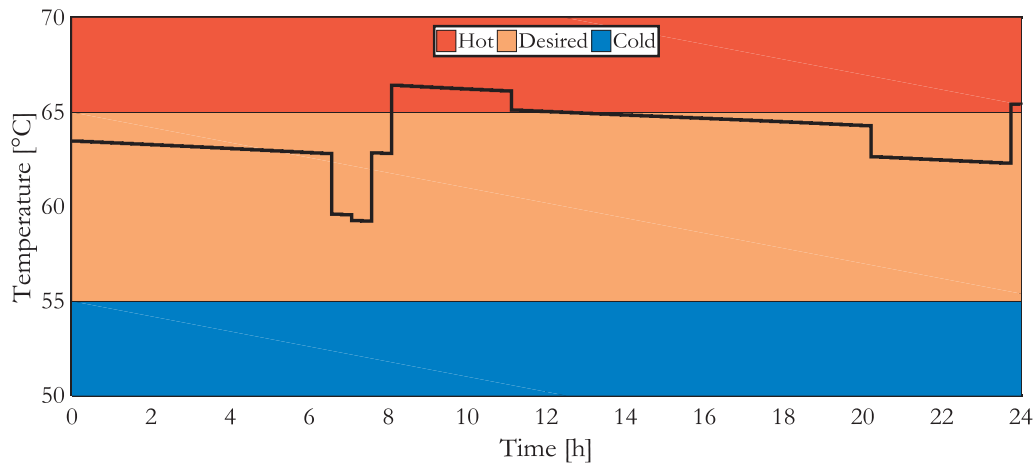**Fig. 13.** Switching function of the ESTWH during winter season (July 2017).

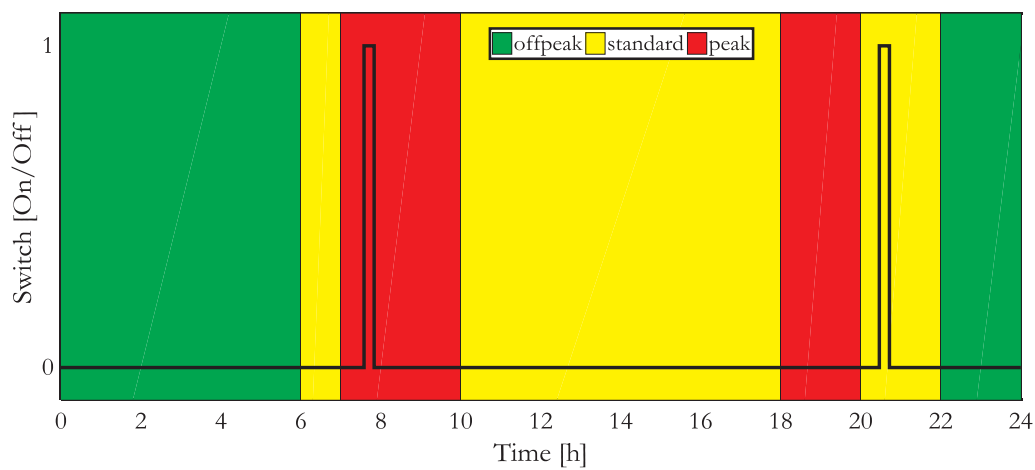**Fig. 14.** Storage tank water temperature of the ESTWH during winter season (July 2017).

Fig. 15. Switching function of the ESTWH during summer season (January 2017).
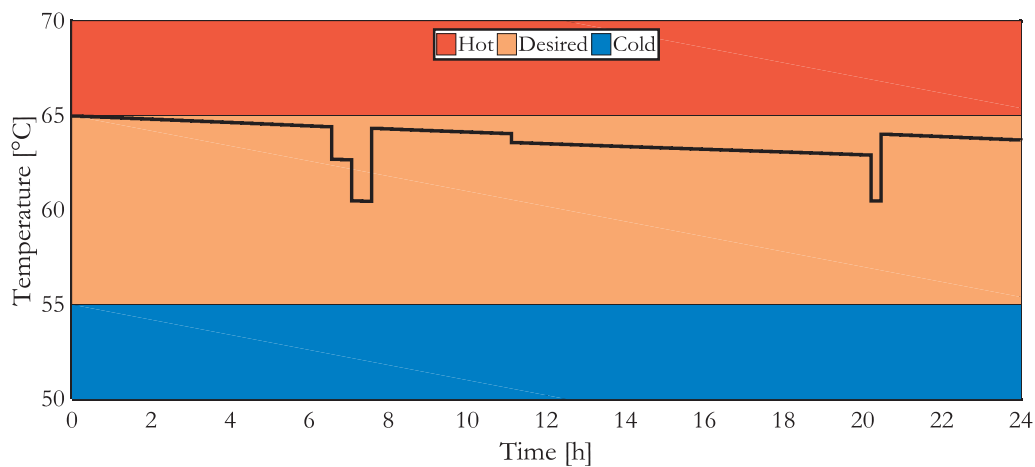

Fig. 16. Storage tank water temperature of the ESTWH during summer season (January 2017).

demand season, particularly by the baseline system. The optimally controlled hybrid system consumed significantly less electrical energy, with the assistance of the solar collector, while using electrical energy solely at the least costly time.

Annual energy consumption and savings

The total cost savings is calculated over the period of one year, by using the data in Table 5. The table presents the energy usage of the

baseline and hybrid systems, as well as the calculated daily and monthly savings. The difference in daily energy costs between the baseline system and the hybrid solar water heater was calculated, in order to obtain the daily savings for each month. The daily savings were multiplied by the number of days in each month, in order to estimate the cumulative energy savings for each respective month. Referring to Table 6, the seasonal costs were calculated based on the monthly costs noted in Table 5. The seasonal costs in the table were added in order to
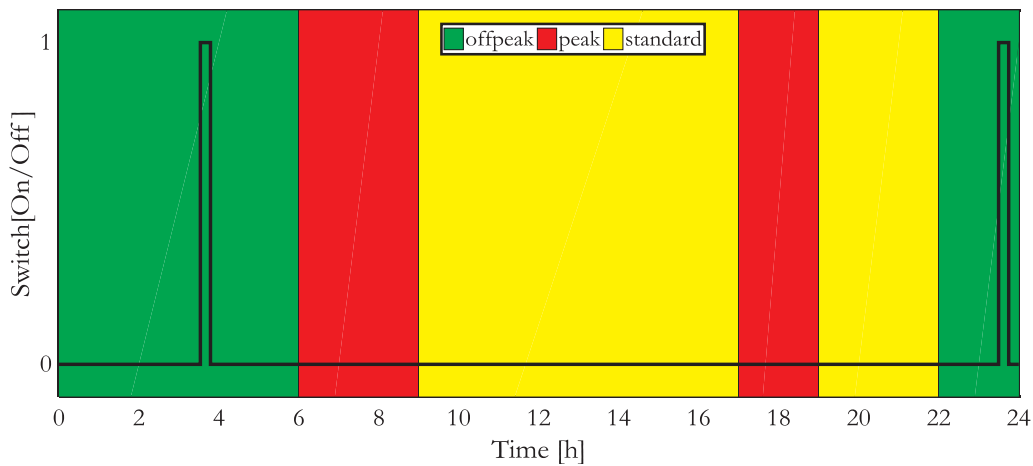
Fig. 17. Optimal switching function of the HSWH during winter season (July 2017).
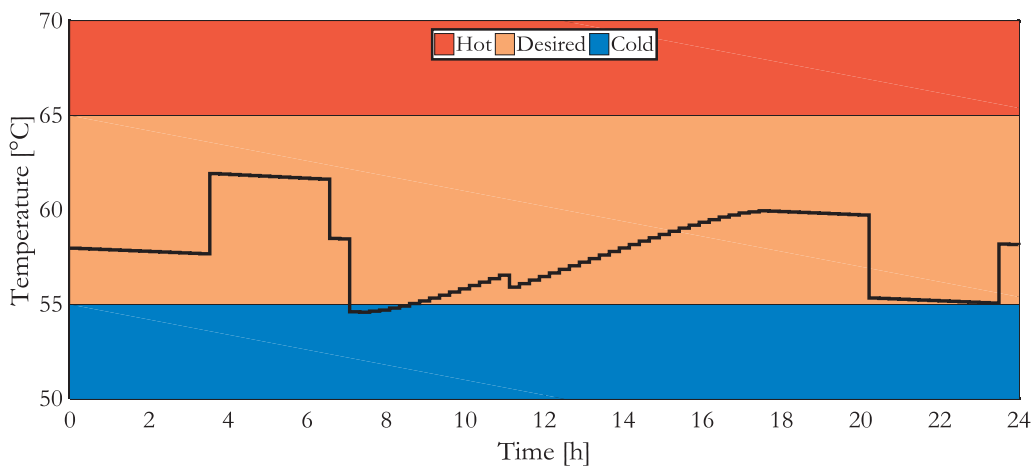

Fig. 18. Optimal storage tank water temperature of the HSWS during winter season (July 2017).
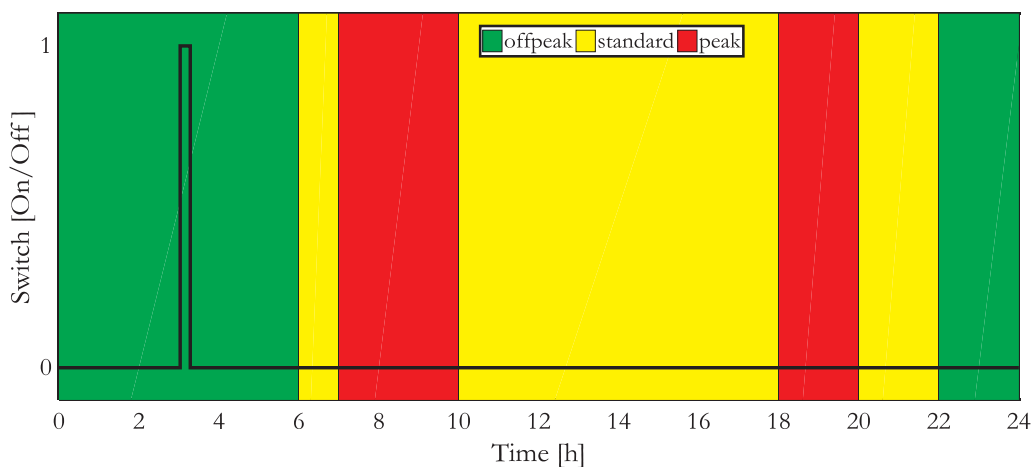

Fig. 19. Optimal switching function of the HSWH during summer season (January 2017).

obtain the average annual energy cosnumptions and savings.

Life cycle cost analysis

In order to reduce the margin of error, a project lifetime of 20 years was determined for the hybrid system. The chosen lifetime is based on the fact that the collector is guaranteed for 10 years, however, several cases have observed the lifetime reaching over 30 years. Hence the

average number of years between guaranteed and actual reported lifespan was chosen.

The replacement cost is calculated using Eq. (40), in Section "Model validation". With the average inflation rate presented in Fig. 24 the future costs of components may be predicted, by assuming that the average inflation rate will be equal to the interest rate [59].

The salvage costs were calculated using Eq. (42), for both the baseline and the hybrid water heating system. This accounts for
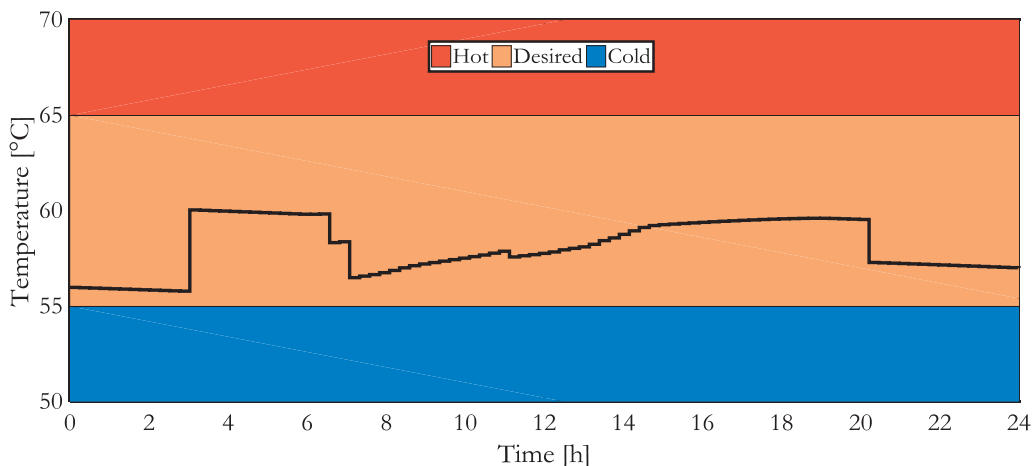
Fig. 20. Storage tank water temperature of the HSWH during summer season (January 2017).

Table 4
Bill of quantity of HSWH.

Component description	Quantity	Net price (ZAR)
150L GAP Eco Electric Storage tank water heater	1	2560.40
150L GAP 2.1 m² Flat Plate Collector	1	4586.80
Geyserwise Max controller	1	1222.08
Air release valve	1	277.00
Circulation pump	1	1425
22 mm thermostatic mixing valve (55 °C)	1	624.15
Labour	-	1500
Eskom rebate	-	− 4677.00
Total initial investment cost	-	7518.43

replacement upgrades to more efficient systems in the future.

Baseline life cycle cost analysis

The total replacement costs (C_{rep}) over the 20-year lifespan for the baseline (ESTWH), are presented in Table 7. The ESTWH has one component, therefore, the total lifecycle replacement costs ($C_{rep-BTC}$) are equal to the replacement costs of the ESTWH.

The total lifecycle cost value LCC_{ESTWH} (ZAR), using Eq. (43), is presented in Table 8. Over a 20 year project lifetime, a total amount of approximately R 110600.99 will be spent, in the case of the ESTWH.

Hybrid system with optimal control life cycle cost analysis

In the case of the hybrid system, several more components exist with various life expectancies, concluding that the total replacement

costs (C_{rep}), calculated using Eq. (40) in Section "Model validation", over the 20 year project lifespan for all the hybrid system's components, presented in Table 9 are added in order to obtain the total lifecycle replacement costs (C_{rep-TC}).

The same method for cumulative electricity costs, with an annual 10% increment, was calculated for the hybrid system, using Eq. (39), as well as for the cumulative operation and maintenance costs and the salvage cost for the HSWH in Eqs. (41) and (42), respectively. Eq. (46) shows the calculation of the lifecycle cost for the HSWH. Table 10 shows the resultant cumulative costs for the HSWH.

The total lifecycle cost value LCC_{HSWH} (ZAR), using Eq. (43), with the data shown in Table 11, is calculated. Over a 20-year project lifetime, a total amount of approximately R 61991.20 will be spent, in the case of the HSWH, with an optimal energy management scheme implemented.

Break-even point (BEP)

The break-even point is determined as the total implementation and operating costs of two systems incurred are equal. In this case, the baseline water heater is compared to the proposed hybrid system, with the optimal energy management scheme, in terms of the total cumulative annual energy cost in the project lifetime of 20 years.

The cumulative cost curves, which includes the initial investment cost and the total annual costs incurred over this period for the baseline and optimal hybrid system, is plotted on the same axis. The intersect point of these two curves shows the point in time (years), at which the two systems break even.
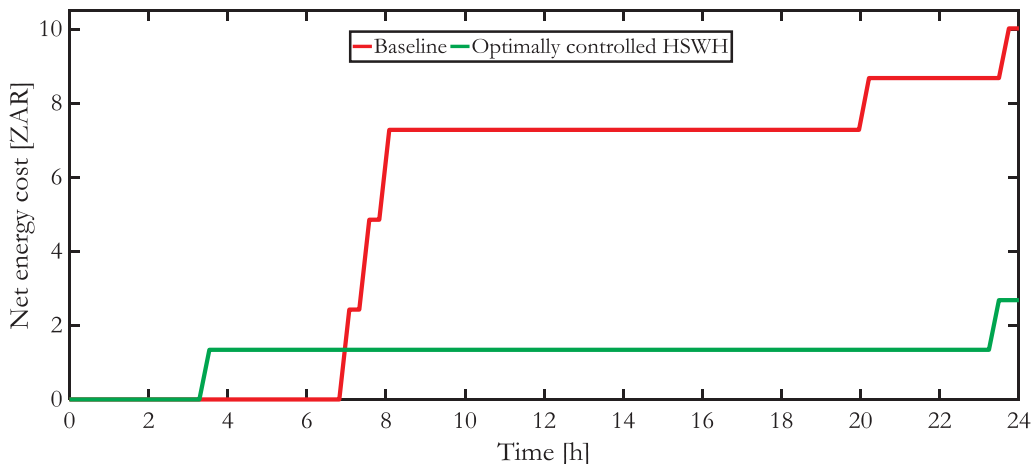

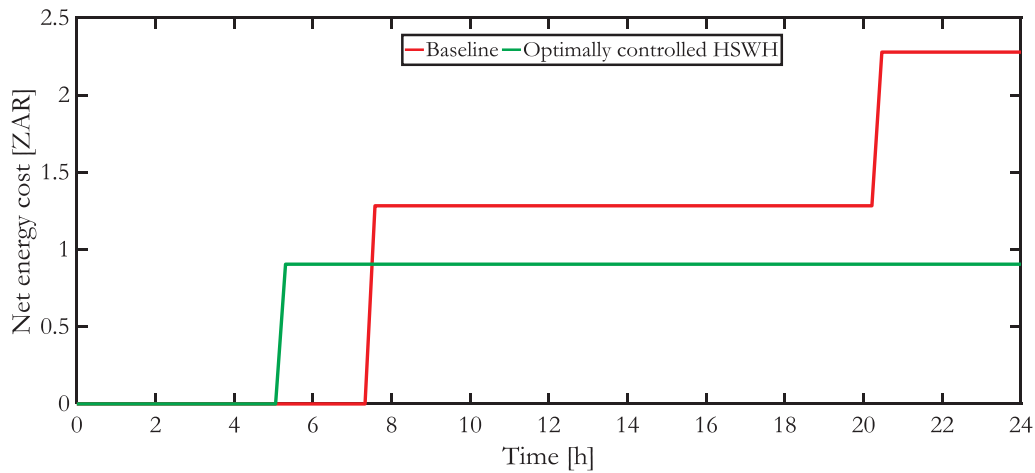**Fig. 21.** Winter cumulative energy cost (July 2017).
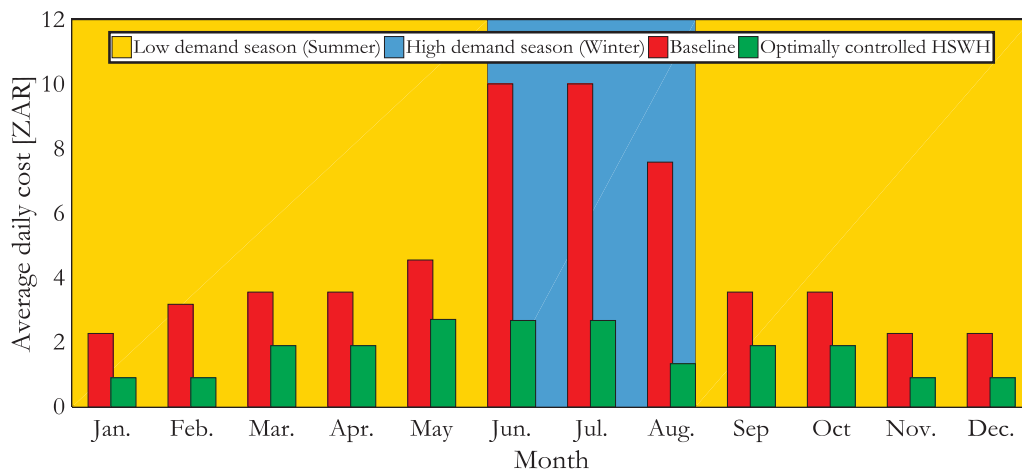
Fig. 22. Summer cumulative energy cost (January 2017).

Fig. 23. Monthly average cumulative energy cost (2017).

Table 5
Daily energy consumption and savings.

Month	Baseline (ESTWH)		Optimal control (HSWH)		Daily Savings		Monthly Savings	
	Energy (kWh)	Cost (ZAR)	Energy (kWh)	Cost (ZAR)	Energy (kWh)	Cost (ZAR)	Energy (kWh)	Cost (ZAR)
January	1.500	2.2783	0.75	0.9047	0.750	1.3736	23.25	42.5816
February	1.500	3.1830	0.75	0.9047	0.750	2.2783	21.00	63.7924
March	1.750	3.5614	1.25	1.8999	0.500	1.6615	15.50	51.5065
April	1.750	3.5614	1.25	1.8999	0.500	1.6615	15.00	49.8450
May	2.000	4.5566	1.75	2.7142	0.250	1.8424	7.75	57.1144
June	3.750	10.018	1.50	2.6813	2.250	7.3366	67.50	220.098
July	3.750	10.018	1.50	2.6813	2.250	7.3366	69.75	227.435
August	3.000	7.5915	1.00	1.3406	2.000	6.2509	62.00	193.778
September	1.750	3.5614	1.00	1.8999	0.750	1.6615	22.50	49.8450
October	1.750	3.5614	1.25	1.8999	0.500	1.6615	15.50	51.5065
November	1.500	2.2783	0.75	0.9047	0.750	1.3736	22.50	41.2080
December	1.500	2.2783	0.75	0.9047	0.750	1.3736	23.25	42.5816

Table 6
Annual energy consumption and savings.

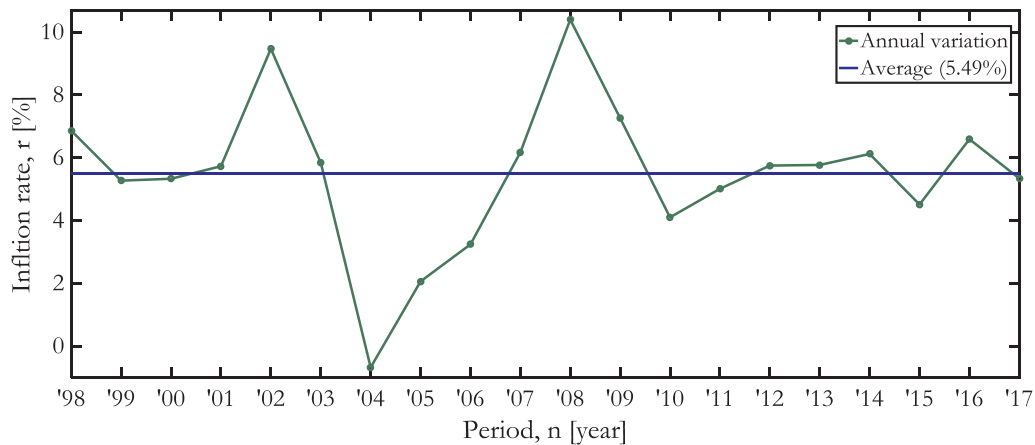| Season	Baseline (ESTWH)		Optimal control (SWH/ESTWH)		Annual Savings (ZAR)	Annual Savings (%)	
	Energy (kWh)	Cost (ZAR)	Energy (kWh)	Cost (ZAR)	Cost	Energy	Cost
Summer	455.50	874.47	289.25	424.49	450.18	36.5	51.5
Winter	321.75	846.42	122.50	205.12	641.30	61.9	75.8
Total	777.25	1720.89	411.75	629.61	**1091.48**	42.9	57.6

Fig. 24. Inflation rate of South Africa from 1998 to 2017 (Adapted from [59].

Table 7
Total replacement cost for the ESTWH.

Parameters	Value
150L GAP ESTWH lifetime (years)	7
$N_{rep-ESTWH}$	2
$C_{rep-ESTWH}$	8072.68
$C_{rep-BTC}$	8072.68

Table 8
Total life cycle cost for the ESTWH.

Cumulative Cost	Value (ZAR)
$C_{initial}$	2560.40
$C_{rep-BTC}$	8072.68
C_{OM}	891.68
C_{EC}	98564.15
$C_{salvage}$	512.08
LCC_{ESTWH}	110600.99

Table 9
Total replacement cost for the SWH/ESTWH.

Parameters	Value
Hybrid system lifetime, n (years)	20
150L GAP FPC lifetime (years)	20
N_{rep-SC} (–)	0
C_{rep-SC} (ZAR)	0
150L GAP ESTWH lifetime (years)	7
$N_{rep-ESTWH}$ (–)	2
$C_{rep-ESTWH}$ (ZAR)	8072.68
Geyserwize Max controller lifetime (years)	7
$N_{rep-CONT}$ (–)	2
$C_{rep-CONT}$ (ZAR)	3853.10
Air release valve (years)	20
$N_{rep-ARV}$ (–)	0
$C_{rep-ARV}$ (ZAR)	0
Circulation pump (years)	12
N_{rep-CP} (–)	1
C_{rep-CP}(ZAR)	2363.79
22 mm thermostatic mixing valve lifetime (years)	20
$N_{rep-TMV}$ (–)	0
$C_{rep-TMV}$ (ZAR)	0
C_{rep-TC} (ZAR)	14289.56

From Table 4, the initial total cost of implementation of the hybrid and the standalone ESTWH is R7518.43 and R2560.40, respectively. These values are, therefore, starting points of the two curves in Fig. 25.

Table 10
Total life cycle cost for the HSWH with optimal scheduling.

Cumulative Cost	Value (ZAR)
$C_{initial}$	7518.43
C_{rep-TC}	14 289.56
C_{OM}	2618.61
C_{EC}	36060.91
$C_{salvage}$	1503.69
LCC_{HSWH}	61991.2

Table 11
Life cycle cost comparison.

LCC	Value (ZAR)
LCC_{ESTWH} (ZAR)	110600.99
LCC_{HSWH} (ZAR)	61991.20
Total savings over 20 years (ZAR)	48 609.79

After the first year has passed, the total annual cost of energy is added to the initial investment cost, which is the total present cost of energy, shown in Table 5. This equates to the total cumulative cost for the first year after implementation. For the second year after implementation, a 10% increase in the price of electricity is taken into account, to calculate the annual energy costs. This amount is once again added to the previous total cumulative cost of the first year. The aforementioned method is followed for years 3 to 10, in Fig. 25. In this curve, the replacement costs and lifetimes of all the components are taken into account, for increased accuracy of cumulative cost representation. From Fig. 25, a clear observation may be made that the break-even point occurs early in the project lifetime. In 3.3 years, the costs incurred are equal at R 10 870 and the differences in total money spent at the end of the project lifetime further present an important economic performance indicator and is discussed in Section "Life cycle cost comparison".

Life cycle cost comparison

The life cycle costs for the traditional electric storage tank water heater, as well as for the hybrid system with optimal energy management scheme, are compared in Table 10. The break-even point analysis concludes the time it will take for cumulative cost equalization. The difference in LCC is calculated, in order to note the savings in costs, at the end of the project lifetime.

From Table 10, a conclusion may be made that in the long run (over the 20-year project lifetime of the system), an approximate saving of R48 609.79 may be made if the HSWH with optimal energy management system, was implemented. This translates into a saving of 44%.
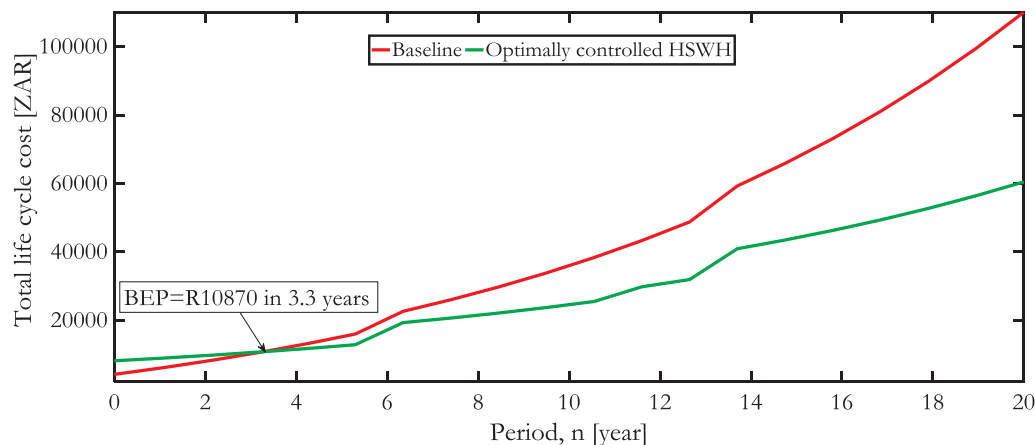
Fig. 25. Break-even point.

Conclusion

In this paper, the cost effectiveness of the hybrid solar/electric water heating system was evaluated. The differences in cumulative energy consumption and costs were noted, henceforth, the annual energy usage and cost savings comparisons could be made.

A break-even point analysis was conducted in order to calculate the time that the proposed system would have an equivalent cumulative cost, compared to the baseline system. The analysis concluded that after 3.3 years, the cumulative costs were lower for the proposed system, as opposed to the baseline. It was observed that after the break-even point, the difference in cumulative costs significantly increased with the baseline cost, following an exponential trend.

The break-even point analysis was followed by a thorough life cycle cost evaluation, ensuring that the savings over a project lifetime of 20 years, could be calculated. The LCC comparison of the proposed system, with respect to the baseline, presented a R48 609.79 saving in cost over the project lifetime. In order to put this in perspective, a saving of 44% in cost was calculated.

Therefore, the LCC analysis validates that the traditional water heating system (baseline), has a lower initial investment cost, yet in the long term, will incur much higher costs, compared to the proposed system.

The LCC calculations for both systems included a relatively low interest rate, which in real terms, may increase the costs of replacements of components, if it were to be higher than the average calculated 5.49%. Furthermore, a 10% increase in electricity cost may further be observed as a conservative assumption, due to the fact that past increments in cost were considerably higher in comparison. With this in mind, it can be said that the calculated 44% saving in cost may be observed as the minimum saving that could be achieved with the proposed system.

Acknowledgements

Appendix A. Supplementary data

Supplementary data to this article can be found online at https://doi.org/10.1016/j.seta.2018.12.027.

References

[1] Qase, N, 2015. State of Renewable Energy in South Africa. 1st ed. Matimba House, 192 Visagie Str, Pretoria, South Africa: Department of Energy.
[2] Gets, A. 2013. Powering the Future: Renewable Energy Roll-out in South Africa. Prepared for Greenpeace Africa by AGAMA Energy (Pty) Ltd Cape Town, South Africa.
[3] Hohne PA, Kusakana K. A survey of domestic water heating technologies.
[4] Eskom. Reduce electricity costs at home. 2015. URL .
[5] Xia Xiaohua, Zhang Jiangfeng, Cass William. Energy management of commercial buildings-a case study from a POET perspective of energy efficiency. J Energy Southern Africa 2012;23(1):23–31.
[6] Lane IE, Beute N. A model of the domestic hot water load. IEEE Trans Power Syst 1996;11(4):1850–5.
[7] Catherine Quinton, Wheeler Jacques, Wilkinson Richardt, de Jager Gerhard. Hot water usage profiling to improve geyser efficiency. J Energy Southern Africa 2012;23(1):39–45.
[8] Chikuni E, Govender T, Okoro OI. A test rig for evaluating the efficiency of hot water boilers under various operating conditions. In Domestic use of energy conference (DUE), 2012 Proceedings of the 20th, pp. 145–152. IEEE, 2012.
[9] Strbac Goran. Demand side management: benefits and challenges. Energy Policy 2008;36(12):4419–26.
[10] Gellings Clark W. The concept of demand-side management for electric utilities. Proc IEEE 1985;73(10):1468–70.
[11] Ghent, Bobby A. Demand side management of water heater systems. U.S. Patent 6, 861,621, issued March 1, 2005.
[12] Harbin III, Benjamin F., Cecil Ray Holland, Robert J. Toth, Adrian O'neil, Michael Scott Sansom, R. Michael Browder, Brook Marin. Water heater demand side management system. U.S. Patent 8,204,633, issued June 19, 2012.
[13] Gelazanskas Linas, Gamage Kelum AA. Demand side management in smart grid: a review and proposals for future direction. Sustainable Cities Soc 2014;11:22–30.
[14] Kaseke Nyasha, Hosking Stephen G. Sub-Saharan Africa electricity supply inadequacy: implications. Eastern Africa Soc Sci Res Rev 2013;29(2):113–32.
[15] Sebitosi AB. Energy efficiency, security of supply and the environment in South Africa: moving beyond the strategy documents. Energy 2008;33(11):1591–6.
[16] Gottwalt Sebastian, Ketter Wolfgang, Block Carsten, Collins John, Weinhardt Christof. Demand side management—a simulation of household behavior under variable prices. Energy policy 2011;39(12):8163–74.
[17] Arteconi Alessia, Hewitt Neil J, Polonara Fabio. State of the art of thermal storage for demand-side management. Appl Energy 2012;93:371–89.
[18] Van Tonder JC, Lane IE. A load model to support demand management decisions on domestic storage water heater control strategy. IEEE Trans Power Systems 1996;11(4):1844–9.
[19] Atikol Uğur. A simple peak shifting DSM (demand-side management) strategy for residential water heaters. Energy 2013;62:435–40.
[20] Energy.gov.za. (2018). [online] Available at: http://www.energy.gov.za/files/aboutus/DoE-Strategic-Plan-2015-2020.pdf [Accessed 7 Apr. 2018].
[21] Pegels Anna. Renewable energy in South Africa: potentials, barriers and options for support. Energy policy 2010;38(9):4945–54.
[22] Mekhilef Saidur, Saidur Rahman, Safari Azadeh. A review on solar energy use in industries. Renew Sustain Energy Rev 2011;15(4):1777–90.
[23] Banos Raul, Francisco Manzano-Agugliaro FG, Montoya Consolacion Gil, Alcayde Alfredo, Gómez Julio. Optimization methods applied to renewable and sustainable energy: a review. Renew Sustain Energy Rev 2011;15(4):1753–66.
[24] Gellings Clark W. Power/energy: demand-side load management: the rising cost of peak-demand power means that utilities must encourage customers to manage power usage. IEEE Spectr 1981;18(12):49–52.
[25] Hohne PA, Kusakana K, Numbi BP. Techno-economic Comparison of Timer and Optimal Switching Control applied to Hybrid Solar Electric Water Heaters.
[26] Lindenberger Dietmar, Bruckner Thomas, Groscurth H-M, Kümmel Reiner. Optimization of solar district heating systems: seasonal storage, heat pumps, and cogeneration. Energy 2000;25(7):591–608.
[27] Koroneos Christopher, Spachos Thomas, Moussiopoulos Nikolaos. Exergy analysis of renewable energy sources. Renewable Energy 2003;28(2):295–310.
[28] Ayompe LM, Duffy Aidan, Mc Keever M, Conlon M, McCormack SJ. Comparative field performance study of flat plate and heat pipe evacuated tube collectors (ETCs) for domestic water heating systems in a temperate climate. Energy 2011;36:3370–8.

[29] Ehrmann N, Reineke-Koch R. Selectively coated high efficiency glazing for solar-thermal flat-plate collectors. Thin Solid Films 2012;520(12):4214–8.

[30] Hohne PA, Kusakana K, Numbi BP. A review of water heating technologies: an application to the South African context. Energy Reports 2019;5:1–19.

[31] McDADE Joseph E, Brenner Don J, Marilyn Bozeman F. Legionnaires' disease bacterium isolated in 1947. Ann. Internal Med. 1979;90(4):659–61.

[32] Wanjiru, Evan M., Sam M. Sichilalu, Xiaohua Xia. Optimal integrated diesel grid-renewable energy system for hot water devices. Energy Procedia 103 (2016): 117–122. Ko, Myeong Jin. A novel design method for optimizing an indirect forced circulation solar water heating system based on life cycle cost using a genetic algorithm. Energies 8, no. 10 (2015): 11592–11617.

[33] Hohne PA, Kusakana K, Numbi BP. Operation cost minimisation of hybrid solar/electrical water heating systems: model development. Adv. Sci. Lett. 2018;24(11):8076–80.

[34] Giglmayr Sebastian, Brent Alan C, Gauché Paul, Fechner Hubert. Utility-scale PV power and energy supply outlook for South Africa in 2015. Renewable Energy 2015;83:779–85.

[35] Atia Doaa M, Fahmy Faten H, Ahmed Ninet M, Dorrah Hassen T. Optimal sizing of a solar water heating system based on a genetic algorithm for an aquaculture system. Math Comput Modell 2012;55(3):1436–49.

[36] Sichilalu Sam, Mathaba Tebello, Xia Xiaohua. Optimal control of a wind–PV-hybrid powered heat pump water heater. Appl Energy 2015.

[37] Hohne PA, Kusakana K, Numbi BP. Operation cost and energy usage minimization of a hybrid solar/electrical water heating system. In 2018 international conference on the domestic use of energy (DUE), pp. 1–7. IEEE, 2018.

[38] EE Publishers. (2017). Energy management systems save money – EE Publishers. [online] Available at: http://www.ee.co.za/article/energy-management-systems-save-money.html [Accessed 8 Dec. 2017].

[39] Hohne, Percy A, Kanzumba Kusakana, Bubele P Numbi. Optimal Energy Management and Economic Analysis of a Grid-Connected Hybrid Solar Water Heating System in Bloemfontein. In 2018 IEEE PES/IAS PowerAfrica, pp. 515–520. IEEE, 2018.

[40] Kusakana, Kanzumba. Optimal operation control of hybrid renewable energy systems. PhD diss., Bloemfontein: Central University of Technology, Free State, 2015.

[41] Bratley Paul, Fox Bennet L, Schrage Linus E. A guide to simulation. Springer Science & Business Media 2011.

[42] Hohne PA, Kusakana K, Numbi BP. Scheduling and economic analysis of hybrid solar water heating system based on timer and optimal control. J Storage Mater 2018;20:16–29.

[43] Ko Myeong Jin. Multi-objective optimization design for indirect forced-circulation solar water heating system using NSGA-II. Energies 2015;8(11):13137–61.

[44] Setlhaolo Ditiro, Xia Xiaohua, Zhang Jiangfeng. Optimal scheduling of household appliances for demand response. Electr Power Syst Res 2014;116:24–8.

[45] Sauran.net. (2017). Station Details – Southern African Universities Radiometric Network. [online] Available at: http://www.sauran.net/ShowStation.aspx?station=7 [Accessed 8 Dec. 2017].

[46] Ratikane, Mosepeli. Quality of drinking water sources in the Bloemfontein area of the Mangaung Metropolitan Municipality. PhD diss., Bloemfontein: Central University of Technology, Free State, 2013.

[47] Meyer JP, Tshimankinda M. Domestic hot-water consumption in South African apartments. Energy 1998;23(1):61–6.

[48] Eskom Rebates For Solar Water Heating Systems GeoSolar Geo Group, Geogroup.co.za, 2017. [Online]. Available at: http://www.geogroup.co.za/solar-heating/solar-water-heating-systems/eskom-solar-heating-rebates. [Accessed: 08-Dec-2017].

[49] 150L GAP ECO ELECTRIC GEYSERS, Solar Advice, 2017. [Online]. Available: https://solaradvice.co.za/product/150l-gap-eco-electric-geyser/. [Accessed: 08-Dec-2017].

[50] Sun & moon times today, Bloemfontein, South Africa, Timeanddate.com, 2017. [Online]. Available: https://www.timeanddate.com/astronomy/south-africa/bloemfontein. [Accessed: 08-Dec-2017].

[51] Solar Radiation on a Tilted Surface | PVEducation, Pveducation.org, 2017. [Online]. Available: http://www.pveducation.org/pvcdrom/properties-sunlight/solar-radiation-tilted-surface. [Accessed: 08-Dec-2017].

[52] Eskom.co.za, 2017. [Online]. Available: http://www.eskom.co.za/CustomerCare/TariffsAndCharges/Documents/Tariff%20book%202018-2018.pdf. [Accessed: 08-Dec-2017].

[53] Cms.centlec.co.za, 2017. [Online]. Available: http://cms.centlec.co.za/documents/CENTLEC%20Southern%20Free%20State%20Tariff%20Approval%20Letter%20201718.pdf. [Accessed: 08-Dec-2017].

[54] Harris A, Kilfoil M, Uken EA. Domestic energy savings with geyser blankets. (2007).

[55] Numbi BP, Malinga SJ. Optimal energy cost and economic analysis of a residential grid-interactive solar PV system-case of eThekwini municipality in South Africa. Appl Energy 2017;186:28–45.

[56] Geogroup.co.za. (2017). Eskom Rebates For Solar Water Heating Systems | GeoSolar | Geo Group. [online] Available at: http://www.geogroup.co.za/solar-heating/solar-water-heating-systems/eskom-solar-heating-rebates [Accessed 21 Dec. 2017].

[57] Garden H, Equipment T, Hardware D, Geysers G. (2017). Gap 150l Eco Electric Geysers | R2245.97 | DIY Hardware | PriceCheck SA. [online] Pricecheck.co.za. Available at: https://www.pricecheck.co.za/offers/89825039/Gap+150l+Eco+Electric+Geysers [Accessed 21 Dec. 2017].

[58] G. Unit, 1 Price For Geyserwise Max | PriceCheck South Africa, Pricecheck.co.za, 2017. [Online]. Available: https://www.pricecheck.co.za/search?search=geyserwise+max. [Accessed: 21-Dec-2017].

[59] T. Media, "Historic inflation South Africa – historic CPI inflation South Africa", Inflation.eu, 2017. [Online]. Available: http://www.inflation.eu/inflation-rates/south-africa/historic-inflation/cpi-inflation-south-africa.aspx. [Accessed: 08-Dec-2017].